Article

Cell Reports

MTA2/NuRD Regulates B Cell Development and Cooperates with OCA-B in Controlling the Pre-B to Immature B Cell Transition

Graphical Abstract

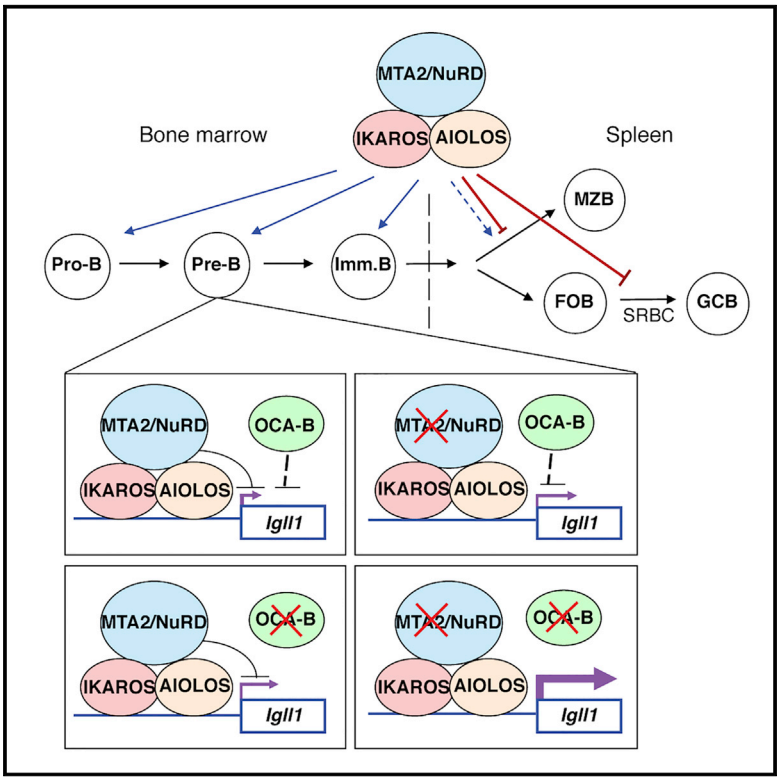

Highlights

- Loss of MTA2 causes bone marrow and splenic B cell developmental defects in mice
- Loss of MTA2 causes derepression of *Igll1* and *VpreB1* genes in pre-B cells
- MTA2 binding sites highly overlap AIOLOS/IKAROS binding sites in pre-B cells
- MTA2 cooperates with OCA-B in regulating pre-B to immature B transition

Authors

Xiangdong Lu, Chi-Shuen Chu, Terry Fang, ..., Yi Zhang, F. Nina Papavasiliou, Robert G. Roeder

Correspondence

roeder@rockefeller.edu

In Brief

Lu et al. examine B cell developmental defects in MTA2-deficient mice. MTA2 interacts with AIOLOS/IKAROS, represses *Igll1* expression, co-binds to most AIOLOS/IKAROS target genes in pre-B cells, and cooperates with OCA-B in the pre-B to immature B transition. These data suggest that AIOLOS/IKAROS functions through MTA2/NuRD during B cell development.

Lu et al., 2019, Cell Reports *28*, 472–485
July 9, 2019
https://doi.org/10.1016/j.celrep.2019.06.029

CellPress

OPEN ACCESS
CellPress

Cell Reports
Article

MTA2/NuRD Regulates B Cell Development and Cooperates with OCA-B in Controlling the Pre-B to Immature B Cell Transition

Xiangdong Lu,[1] Chi-Shuen Chu,[1] Terry Fang,[2] Violeta Rayon-Estrada,[3] Fang Fang,[4] Alina Patke,[2] Ye Qian,[5] Stephen H. Clarke,[5] Ari M. Melnick,[4] Yi Zhang,[6] F. Nina Papavasiliou,[3,7] and Robert G. Roeder[1,8,*]

[1]The Laboratory of Biochemistry and Molecular Biology, The Rockefeller University, New York, NY 10065, USA
[2]The Laboratory of Immune Cell Epigenetics and Signaling, The Rockefeller University, New York, NY 10065, USA
[3]The Laboratory of Lymphocyte Biology, The Rockefeller University, New York, NY 10065, USA
[4]Department of Medicine, Division of Hematology and Medical Oncology, Weill Cornell Medicine, New York, NY 10065, USA
[5]Department of Microbiology and Immunology, University of North Carolina at Chapel Hill, Chapel Hill, NC 27599, USA
[6]HHMI, Boston Children's Hospital, Harvard Medical School, Boston, MA 02115, USA
[7]Division of Immune Diversity, German Cancer Research Center (DKFZ), 69120 Heidelberg, Germany
[8]Lead Contact
*Correspondence: roeder@rockefeller.edu
https://doi.org/10.1016/j.celrep.2019.06.029

SUMMARY

The NuRD complex contains both chromatin remodeling and histone deacetylase activities. Mice lacking the MTA2 subunit of NuRD show developmental defects in pro-B, pre-B, immature B, and marginal zone B cells, and abnormal germinal center B cell differentiation during immune responses. *Mta2* inactivation also causes a derepression of *Igll1* and *VpreB1* genes in pre-B cells. Furthermore, MTA2/NuRD interacts directly with AIOLOS/IKAROS and shows a striking overlap with AIOLOS/IKAROS target genes in human pre-B cells, suggesting a functional interdependence between MTA2/NuRD and AIOLOS. Mechanistically, MTA2 deficiency in mice leads to increased H3K27 acetylation at both *Igll1* and *VpreB1* promoters. Gene profiling analyses also identify distinct MTA2-dependent transcription programs in pro-B and pre-B cells. In addition, we find a strong synergy between MTA2 and OCA-B in repressing *Igll1* and *VpreB1* at the pre-B cell stage, and in regulating both the pre-B to immature B transition and splenic B cell development.

INTRODUCTION

Mammalian B lymphocyte development is a tightly regulated multi-step process that proceeds from hematopoietic stem cells (HSCs) in the bone marrow through several intermediate progenitor cell stages, including multipotent progenitors (MPPs), earliest lymphocyte progenitors (ELPs), and common lymphoid progenitors (CLPs), before differentiation into B cells. Intensive studies over the past decades have implicated multiple key transcription factors (TFs) in the regulation of B cell development, including factors (e.g., PU.1, Ikaros, BCL11a, E2A, EBF, and -PAX5) that act either positively to promote B cell-specific gene expression or negatively to repress non-B lineage programs (Busslinger, 2004; Matthias and Rolink, 2005). These sequence-specific TFs achieve activation or repression of target genes through interactions both with the general transcription machinery and with chromatin regulators (e.g., histone modification enzymes and chromatin remodeling complexes), but how specific chromatin regulators contribute to B cell development remains largely unknown (Busslinger and Tarakhovsky, 2014).

Among chromatin-modifying factors, the heterogeneous NuRD (nucleosome remodeling histone deacetylase) complex is of special interest because it possesses both ATP-dependent nucleosome remodeling and histone deacetylase activities. The mammalian NuRD complexes are composed of both common factors (HDAC1/2, RbAp46/48) and variable modular factors that result in related heterogeneous complexes that likely modulate different transcriptional programs (Dege and Hagman, 2014; Feng and Zhang, 2003). Thus, beyond the common components, NuRD complexes variably contain a member (either CHD3/MI-2α or CHD4/MI-2β) of the CHD family of ATP-dependent chromatin remodeling factors, a member (MTA1, MTA2, or MTA3) of the metastasis-associated factor MTA family, a member (MBD2 or MBD3) of the methyl-CpG binding domain proteins, and either P66α or P66β (whose functions are likely to be mediated through interactions with core histones and MBD2) (Dege and Hagman, 2014; Denslow and Wade, 2007). *In vivo* and cell-based studies have demonstrated important and non-redundant functions of different NuRD modular components in multiple biological processes that include embryonic stem cell (ESC) maintenance, tumor progression, circadian clock regulation, synaptic differentiation, and granule neuron function in the cerebellum cortex (Dege and Hagman, 2014; Denslow and Wade, 2007; Kim et al., 2014; Sen et al., 2014; Yamada et al., 2014; Yang et al., 2016).

In relation to NuRD function in lymphogenesis, of primary interest here, previous studies have demonstrated (1) an association of MI-2β/NuRD with IKAROS and AIOLOS in T cells (Avitahl et al., 1999; Zhang et al., 2011); (2) reductions in $CD4^+$ T cell number and *Cd4* gene expression (Williams et al., 2004); (3) abnormal

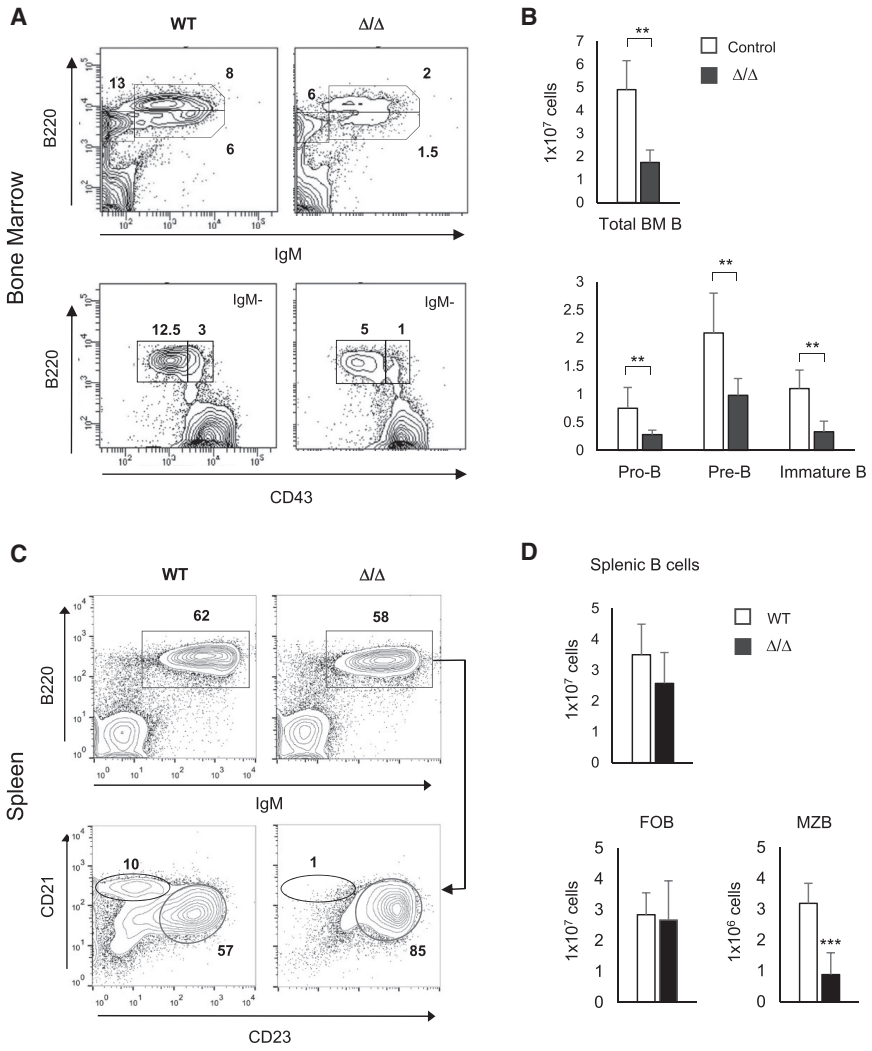

Figure 1. BM and Peripheral B Cell Developmental Defects in the Conventional *Mta2* Null Mice

(A) Flow cytometry data of BM cells from a 2-month-old *Mta2* Δ/Δ and a littermate wild type control mouse stained for immature B ($B220^{lo}IgM^{+}$), mature B ($B220^{hi}IgM^{+}$), pro-B ($B220^{+}IgM^{-}CD43^{+}$), and pre-B ($B220^{+}IgM^{-}CD43^{-}$) cell populations. Numbers indicate percentages of specific cell subsets in parental populations.

(B) Cell numbers of different BM B cell subpopulations (from two femurs) in 1.5- to 2.5-month-old control and *Mta2* Δ/Δ mice (n = 11 for control and n = 5 for mutant mice; t test; *p < 0.05, **p < 0.01, ***p < 0.001).

(C) FACS analysis of total splenic B ($IgM^{+}B220^{+}$), MZB ($IgM^{+}B220^{+}CD21^{hi}CD23^{lo}$), and FOB ($IgM^{+}B220^{+}CD21^{-}CD23^{hi}$) cells from a 4-month-old *Mta2* Δ/Δ mouse and a wild-type (WT) littermate control mouse.

(D) Numbers of total splenic B, MZB, and FOB cells from 2- to 4-month-old wild-type and *Mta2* Δ/Δ mice are plotted (n = 10 for each genotype; t test; ***p < 0.001).

HSC homeostasis and defective differentiation into myeloid and lymphoid lineages (Yoshida et al., 2008), following *Mi-2β* inactivation; (4) an MI-2β requirement for maintaining DNA-hypermethylated chromatin at the *mb1* gene promoter (Gao et al., 2009); (5) spontaneous B cell lymphomagenesis following *Mta1* overexpression *in vivo* (Bagheri-Yarmand et al., 2007); (6) an important role for *Mta3* in plasma cell differentiation (Fujita et al., 2004); and (7) MBD3/NuRD-mediated repression of the B cell transcription program in multipotent lymphoid progenitors in order to maintain a balanced differentiation of T and B lineage cells (Loughran et al., 2017). Related, our previous data showed that *Mta2*-deficient mice develop lupus-like autoimmune symptoms (Lu et al., 2008). However, the role of distinct NuRD complexes in normal B cell development and the transcriptional programs they regulate remain to be elucidated.

Here, we have characterized a number of conventional, conditional mutant and double-mutant mouse models in order to delineate specific phenotypes in B cell development, allowing us to link the MTA2 component of the MTA2/NuRD complex to the lymphocyte-specific transcription factor AIOLOS and the B cell-specific transcription coactivator OCA-B (Luo and Roeder, 1999; Teitell, 2003) *in vivo*. We also identified distinct groups of genes regulated by MTA2 in pro-B and pre-B cells.

RESULTS

B Cell Developmental Defects in *Mta2* Conventional and Conditional Knockout (KO) Mice

To understand the function of MTA2/NuRD in B cell development, we first analyzed the bone marrow (BM) B cell subpopulations in 1.5- to 2.5-month-old *Mta2* conventional null (Δ/Δ) (n = 5) and littermate control mice that include both wild type and *Mta2* heterozygous mice (n = 11). The *Mta2* null strain was derived by crossing *EIIa-Cre* transgenic mice with $Mta2^{fl/fl}$ mice (Lu et al., 2008). *Mta2* null mice showed decreased frequencies of immature B ($B220^{lo}IgM^{+}$), mature B ($B220^{hi}IgM^{+}$), pro-B (also called pre-BI, $B220^{+}IgM^{-}CD43^{+}$), and pre-B (also called pre-BII, $B220^{+}IgM^{-}CD43^{-}$) cells in BM (Figure 1A). On average, the absolute numbers of total BM B ($B220^{+}$), pro-B, pre-B, and immature B cells in *Mta2* Δ/Δ mice were about one-third to one-half of those in control mice (Figure 1B). Regarding the B cell repertoire in the periphery, and while a decrease of marginal zone B (MZB) cells ($IgM^{+}B220^{+}CD21^{hi}CD23^{lo}$) has been observed in young *Mta2* Δ/Δ mice (6–8 weeks), this defect is more consistent and severe in mice older than 3 months old (Figures 1C and 1D). The number of follicular B (FOB) cells ($IgM^{+}B220^{+}CD21^{-}CD23^{hi}$) in adult *Mta2* Δ/Δ mice remains largely normal (Figures 1C and 1D).

To avoid the experimental obstacle caused by partial embryonic lethality of *Mta2* Δ/Δ mice (Lu et al., 2008) and,

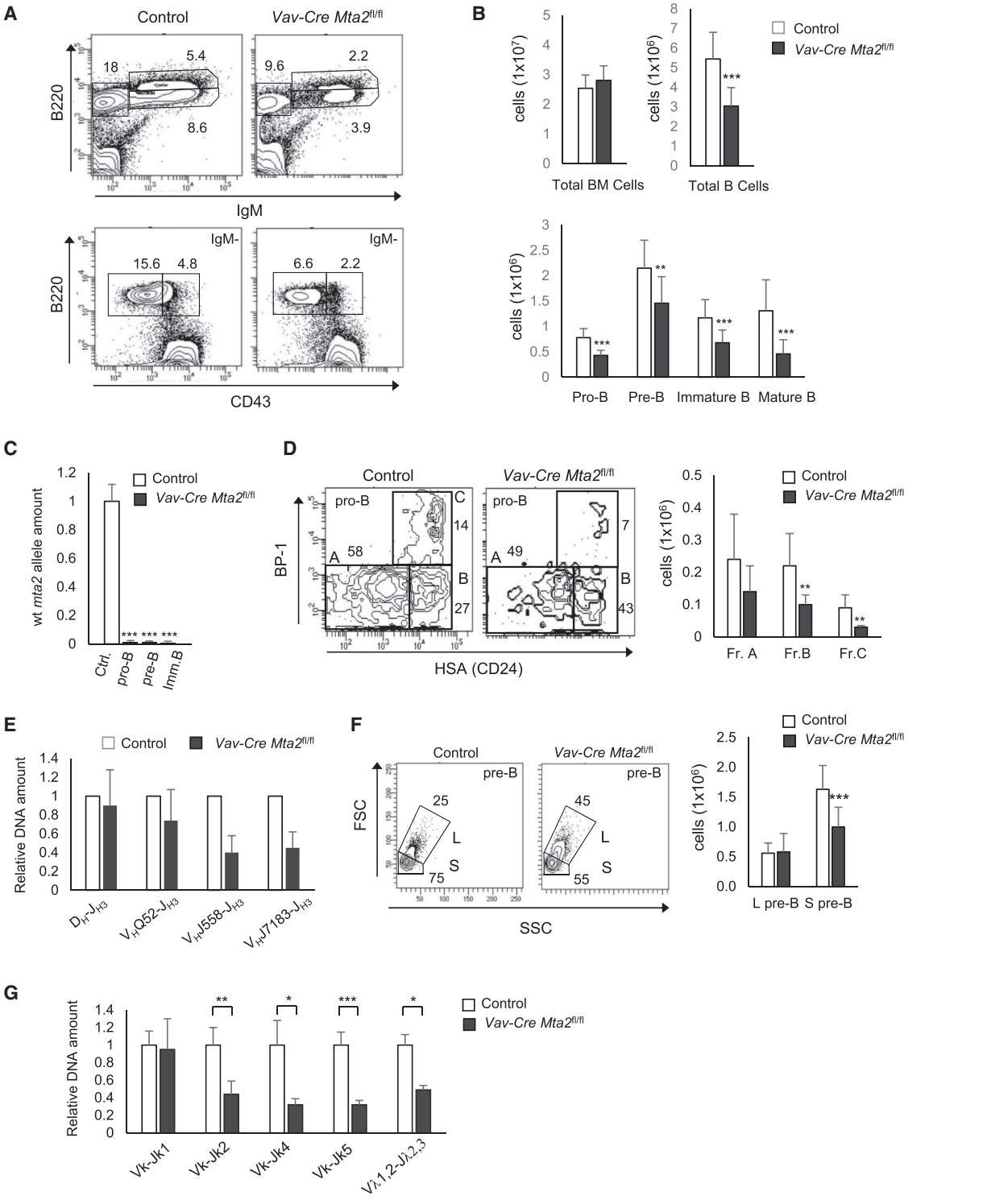

Figure 2. *Vav-Cre Mta2*$^{fl/fl}$ Mice Recapitulate the BM B cell Developmental Defects of *Mta2*Δ/Δ Mice

(A) BM cells from mice with indicated *Mta2* status stained for immature B (B220^{lo}IgM^{+}), mature B (B220^{hi}IgM^{+}), pro-B (B220^{+}IgM^{-}CD43^{+}), and pre-B (B220^{+}IgM^{-}CD43^{-}) cell populations. Numbers indicate percentages of specific cell subsets in parental populations.

(B) Cell numbers of different BM B cell subsets (from two femurs) in 2- to 3-month-old *Vav-Cre Mta2*$^{fl/fl}$ and littermate or age-matched control mice ($n \geq 16$ for *Vav-Cre Mta2*$^{fl/fl}$ and control mice; t test; $^{**}p < 0.01$, $^{***}p < 0.001$).

(C) qPCR results indicating efficiencies of Vav-Cre-mediated deletion of *Mta2* allele in indicated cell populations ($n = 4$ for each cell subsets; t test; $^{***}p < 0.001$).

(legend continued on next page)

more importantly, to assess the B cell-autonomous defects, we generated *Cd19-Cre*- and *Mb1-Cre* (*Cd79a*) *Mta2* conditional KO mice. These *Mta2* conditional KO mice were backcrossed with C57/BL6 mice for at least six generations. *Cd19* encodes a B cell-specific cell surface signaling molecule, CD19, that is presented on all $B220^+CD43^+HSA^+$ cells (a mixture of pro-B and large pre-B cells), but not on the earliest B220-expressing cells ($B220^+CD43^+HSA^-$) (Krop et al., 1996). *Mb1* encodes the Igα subunit of the pre-BCR (B cell receptor) complex and is expressed earlier in development than *Cd19* (Hobeika et al., 2006). Surprisingly, fluorescence-activated cell sorting (FACS) analysis showed largely normal pro-B and pre-B cell compartments in *Cd19-Cre Mta2*$^{fl/fl}$ and *Mb1-Cre Mta2*$^{fl/fl}$ mice (Figures S1A–S1C). Subsequent qPCR data revealed that more than 85% of the pro-B cells from *Cd19-Cre Mta2*$^{fl/fl}$ mice and 30% of the pro-B cells from *Mb1-Cre Mta2*$^{fl/fl}$ mice still maintain the wild-type *Mta2* alleles (Figure S1D), partially explaining the lack of pro-B phenotype in these mutant mice. In contrast, both pre-B and immature B cells from *Cd19-Cre Mta2*$^{fl/fl}$ mice, especially those B cell subsets from *Mb1-Cre Mta2*$^{fl/fl}$ mice, show high deletion efficiencies of the *Mta2* allele (Figure S1D). Intriguingly, in relation to splenic B cell development, while *Mta2* Δ/Δ mice show loss of MZB cells, both *Cd19-Cre Mta2*$^{fl/fl}$ and *Mb1-Cre Mta2*$^{fl/fl}$ show increases in MZB cell numbers and MZB frequencies in total spleen cells (Figure S2). To avoid the complexity caused by escaper pro-B cells (cells maintaining the floxed *Mta2* allele) in *Cd19-Cre Mta2*$^{fl/fl}$ and *Mb1-Cre Mta2*$^{fl/fl}$ mice, we generated *Vav-Cre Mta2*$^{fl/fl}$ mice in which *Cre* transgene expression begins at the HSC stage (Ogilvy et al., 1999). FACS analyses revealed decreased population sizes of pro-B, pre-B, immature B cell, and recirculating B cell compartments in *Vav-Cre Mta2*$^{fl/fl}$ mice, thus recapitulating the BM B cell defects of conventional null mice (Figures 2A and 2B) and supporting the notion that *Mta2* is required for normal development of pro-B cells. qPCR results also show optimal deletion efficiencies in different BM B cell subsets (Figure 2C). Within the pro-B cell population, there is more than 50 percent reduction in both Hardy Fractions B (Fr. B) and C (Fr. C) cells when MTA2 is lost (Figure 2D). qPCR analyses show that *Mta2* inactivation results in abnormal rearrangement of immunoglobulin (*Ig*) heavy chain genes (such as V_HJ558-J_{H3} and V_HJ7183-J_{H3}) in pro-B cells (Figure 2E). Regarding the pre-B cell population, *Vav-Cre Mta2*$^{fl/fl}$ mice contain a higher percentage of large pre-B cells and fewer small pre-B cells than control mice (Figure 2F), suggesting a cell cycle defect in these mutant pre-B cells (which might explain the decreased number of immature B cells in mutant mice). In addition, we also find abnormal Ig κ chain rearrangements in *Vav-Cre Mta2*$^{fl/fl}$ small pre-B cells (Figure 2G). Furthermore, the distal recombination events seem to be more affected by *Mta2* inactivation than are the proximal recombination events, suggesting a premature termination of the recombination process (Figure 2G).

MTA2/NuRD-AIOLOS/IKAROS Interaction and MTA2-Dependent Repression of Pre-BCR Genes

Altogether, the B cell phenotypes described above, as well as other defects of the immune system caused by *Mta2* inactivation (Lu et al., 2008), were reminiscent of those found in mice lacking AIOLOS, a member of the IKAROS family and a key regulator of lymphocyte function (Wang et al., 1998). IKAROS and AIOLOS were found to be stably associated with NuRD complexes in T cells (Kim et al., 1999; Zhang et al., 2011). To assess whether MTA2/NuRD interacts with AIOLOS in B cells, nuclear extracts (NEs) from human pre-B leukemia 697 cells were subjected to immunoprecipitation with antibodies to MTA2, MI-2β, AIOLOS, and IKAROS (Figure 3A). The results show reciprocal co-immunoprecipitation between AIOLOS, IKAROS, and NuRD components MTA2 and MI-2β (Figure 3A), and were confirmed with NE from Namalwa cells (of germinal center origin) (Figure S3A). Thus, both phenotypic similarities and direct biochemical evidence suggested that *Mta2*-deficient mice may have other B cell developmental defects similar to those observed in *Aiolos* KO mice.

During mouse BM B cell development, immunoglobulin heavy chain (IgM) rearrangement occurs at the pro-B stage. The heavy chain then associates with the surrogate light chain (SLC), composed of LAMBDA5 (λ5) and VPREB proteins. *Aiolos* expression is upregulated at the pro-B to pre-B cell transition stage, and *Igll1* (encoding λ5) and *VpreB1* genes are downregulated at the pre-B stage. In *Aiolos*-null pre-B cells, both *Igll1* and *Vpreb1* are derepressed—demonstrating a key role of Aiolos in silencing these genes at this stage (Karnowski et al., 2008; Thompson et al., 2007). In addition, *Ikaros* overexpression in mouse pre-B cells also results in decreased *Igll1* expression (Ferreirós-Vidal et al., 2013). To test whether MTA2 is also involved in pre-BCR gene silencing, we examined *Igll1* and *VpreB1* expression levels in small pre-B cells ($B220^+IgM^-CD43^-$) sorted from *Vav-Cre Mta2*$^{fl/fl}$ and control mice (Figure S3B). The RT-qPCR results show marked increases in expression of these genes in *Mta2*-deficient pre-B cells and are confirmed in *Mx1-Cre Mta2*$^{fl/fl}$ pre-B cells (Figure 3B). The increase of *Igll1* and *VpreB1* expression is further confirmed in *Vav-Cre Mta2*$^{fl/fl}$ pre-B cells sorted by an alternative gating scheme ($B220^+IgM^-CD43^-CD25^+$) (Figures S3C and S3D). To examine whether MTA2/NuRD regulates pre-BCR genes directly, chromatin immunoprecipitation (ChIP) assays were performed using 697 human pre-B leukemia cells. The data demonstrate significant enrichments of MTA2, MI-2β, AIOLOS, and IKAROS at *IGLL1* and *VPREB1* promoters (Figure 3C). Thus, both genetic and biochemical experiments clearly demonstrate that MTA2/NuRD directly interacts with AIOLOS and

(D) Representative FACS data showing percentages of Hardy Fr. A to C within the pro-B population in *Vav-Cre Mta2*$^{fl/fl}$ and control mice. The average numbers of each fractions are plotted (n = 9 for each genotype; t test; $^{**}p < 0.01$).
(E) qPCR results indicating relative abundances of different immunoglobulin heavy chain gene rearrangements in pro-B cells isolated from mice with indicated genotypes (n = 4 for each genotype).
(F) Representative FACS data showing percentages of large (L) and small (S) pre-B ($B220^+IgM^-CD43^-$) cells in *Vav-Cre Mta2*$^{fl/fl}$ and control mice. The average numbers of each type of pre-B cells from mice with indicated genotypes are plotted ($n \geq 13$ for *Vav-Cre Mta2*$^{fl/fl}$ and littermate control mice; t test; $^{***}p < 0.001$).
(G) qPCR results indicating relative abundances of different VJ rearrangements in small pre-B cells isolated from mice with indicated genotypes (n = 4 for each genotype; t test; $^{*}p < 0.05$, $^{**}p < 0.01$, $^{***}p < 0.001$).

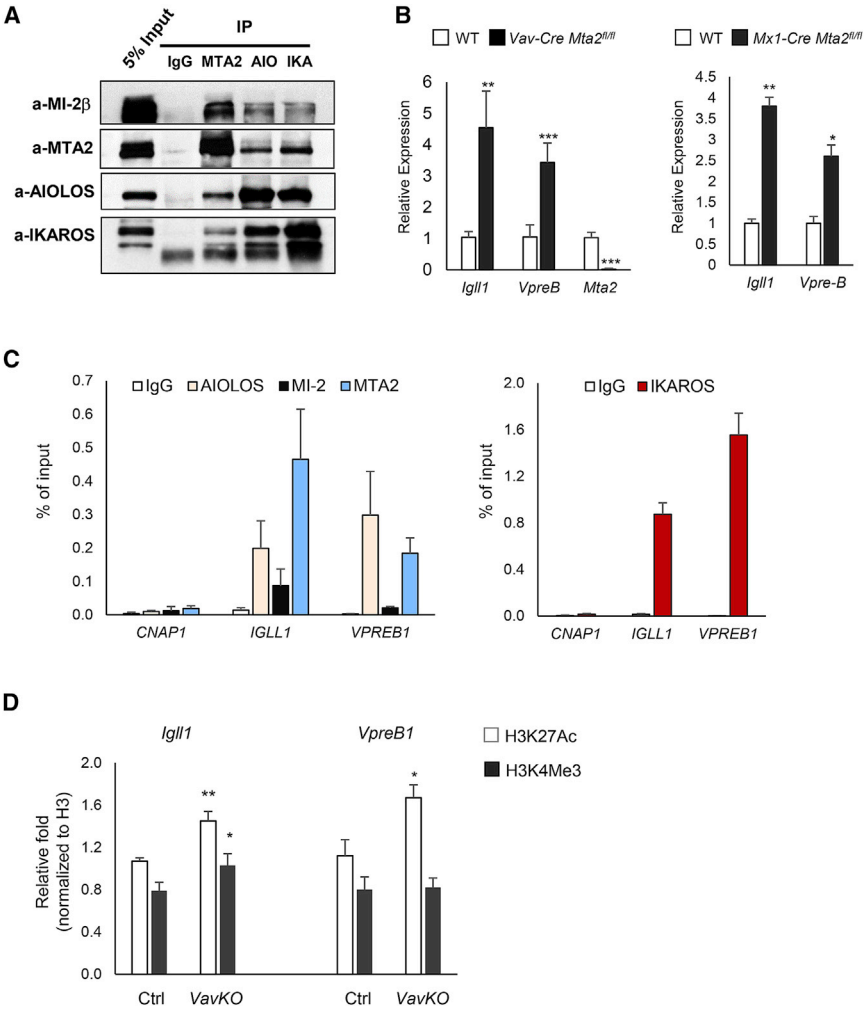

Figure 3. MTA2/NuRD Interacts with AIOLOS and Represses *Igll1* and *VpreB* Genes in Pre-B Cells

(A) Immunoprecipitation (IP)-Western blot results using 697 human pre-B leukemia cell nuclear extract (NE). Antibodies used for IPs and immunoblots are marked (AIO: AIOLOS, IKA: IKAROS).

(B) RT-qPCR results showing expression levels of *Igll1* and *VpreB1* genes in pre-B cells isolated from *Vav-Cre Mta2*$^{fl/fl}$, *Mx1-Cre Mta2*$^{fl/fl}$ and their littermate control mice (n = 4 for *Vav-Cre Mta2*$^{fl/fl}$ and control, n = 3 for *Mx1-Cre Mta2*$^{fl/fl}$ and control; t test; *p < 0.05, **p < 0.01, ***p < 0.001).

(C) ChIP-qPCR data using human 697 cells showing enrichment of AIOLOS, MI-2β, MTA2 (left panel), and IKAROS (right panel) at the *IGLL1* and *VPREB1* promoter regions. The *CNAP1* gene locus was used as a negative region control. Data were collected from 3 or more independent ChIP assays.

(D) ChIP-qPCR data showing enrichment of H3K27Ac and H3K4Me3 marks (normalized to H3) at promoter regions of *Igll1* and *VpreB1* genes in primary small pre-B cells sorted from *Vav-Cre Mta2*$^{fl/fl}$ (*VavKO*) and control mice (t test; *p < 0.05, **p < 0.01).

IKAROS in developing B cells, and jointly targets pre-BCR gene loci. ChIP assays demonstrated that loss of MTA2 activity leads to increase of histone H3 lysine 27 acetylation (H3K27Ac) at both *Igll1* and *VpreB1* promoters (Figure 3D), indicating the mechanism underlying the increased *Igll1* and *Vpreb1* expression in *Mta2*-deficient pre-B cells.

Highly Overlapping Genomic Distributions of MTA2, HDAC2, AIOLOS, and IKAROS in Human Pre-B Cells

To better understand the MTA2/NuRD-dependent gene regulation and its relationship to AIOLOS and IKAROS, we examined the genomic distributions of MTA2, HDAC2 (another subunit of NuRD complex), AIOLOS, and IKAROS in 697 cells by chromatin immunoprecipitation sequencing (ChIP-seq). These analyses identified about 28,760 MTA2 peaks, with 19% at promoter regions, 44% at intragenic regions (including introns, exons, 5′ and 3′ UTR regions), and 34% at intergenic regions (including distal enhancers) (Figure 4A). HDAC2, AIOLOS, and IKAROS showed similar distribution patterns (Figure 4A). A further examination of the average distance from the binding sites of these factors to transcription start sites (TSSs) and enhancers revealed enrichment of all these factors slightly upstream of the TSS (Figure 4B). At enhancer regions, all four factors showed almost the same binding patterns (Figure 4B). Furthermore, the ChIP-seq data showed a striking overlap between target genes bound by these factors (Figure 4C). For example, about 90% of the MTA2 target genes are also AIOLOS targets, more than 90% of the HDAC2 targets are also MTA2 targets, and more than 90% of AIOLOS targets are also IKAROS targets (Figure 4C). A heatmap generated by normalized read densities from individual ChIP-seq data centered at TSSs and ranked by AIOLOS peak signals further demonstrates the high degree of AIOLOS/IKAROS and MTA2/HDAC2 colocalization at promoter regions (Figure 4D). These data strongly support a model in which AIOLOS/IKAROS recruits the MTA2/ NuRD complex to repress target genes in pre-B cells.

Toward the identification of DNA sequence elements recognized by MTA2, HDAC2, AIOLOS, and IKAROS, respectively, motif analyses indicated that the top binding sites preferred by MTA2, HDAC2, and AIOLOS/IKAROS include motifs recognized by EBF1, RUNX1, and ETS family members (FLI1, ERG, and ETV2) (Figure 4E). The more detailed summaries of DNA motifs recognized by these factors are listed in Tables S1–S4. These data suggest a model in which AIOLOS/IKAROS/NuRD function, at least partially, by repressing target genes of EBF1, RUNX1, and ETS family transcription factors in pre-B cells. This notion is consistent with a previously proposed model that AIOLOS represses *Igll1* expression at the pre-B stage by competing with EBF1 at the same DNA binding site (Thompson et al., 2007).

The ChIP-seq data also confirm that the *IGLL1* and *VPREB1* promoters are loaded with AIOLOS and NuRD components MTA2 and HDAC2 (Figure 4F), and that this is also the case for

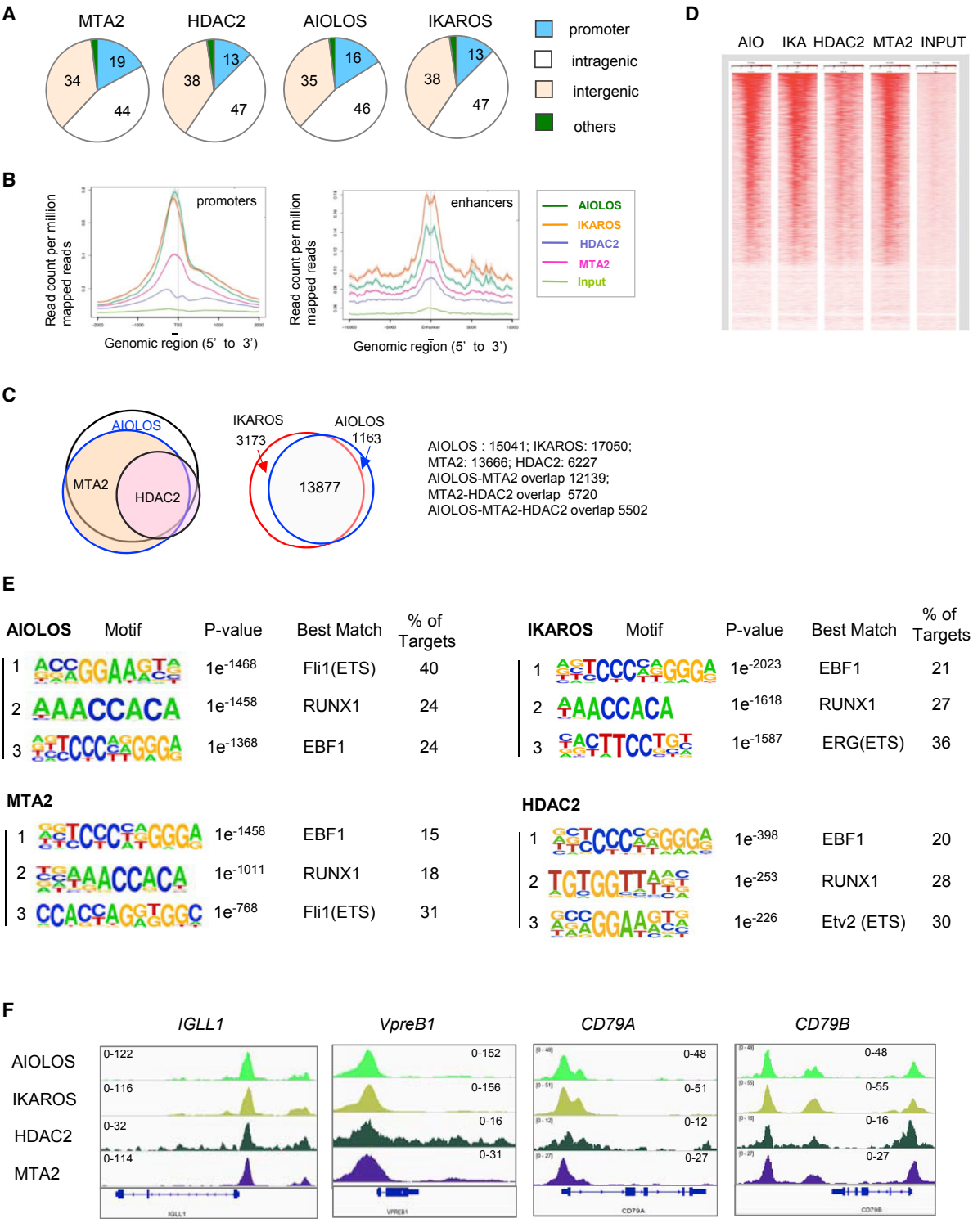

Figure 4. Genome-Wide Mapping of MTA2, HDAC2, AIOLOS, and IKAROS in Human Pre-B Cells

(A) Distribution of MTA2, HDAC2, AIOLOS, and IKAROS binding sites at different genomic locations in 697 human pre-B cells. Numbers indicate the percentage of total sites at each location.

(B) Meta-gene analysis of average enrichment of indicated factors around transcription start sites (TSSs) (left panel) and enhancers (right panel).

(C) Venn diagrams showing significant overlaps between AIOLOS, MTA2, and HDAC2 target genes (left panel) and between IKAROS and AIOLOS target genes (right panel).

(legend continued on next page)

the promoters of the *CD79A* and *CD79B* genes (encoding the Igα and Igβ subunits of the pre-BCR/BCR complexes) (Figure 4F). For a group of genes, such as *CD86* and *BCL2*, AIOLOS/IKAROS and NuRD do not bind to the promoter regions but instead bind to the intronic and 3′ UTR elements (Figures S4A and S4B). Interestingly, the expression levels of *Cd86* and *Bcl2* are elevated in *Mta2*-deficient murine pre-B cells (data not shown), suggesting a possible enhancer-mediated transcription repression for these genes.

MTA2-Dependent Transcriptional Program in Pro-B and Pre-B Cells

To understand the molecular basis of pro-B and pre-B defects observed in *Vav-Cre Mta2*$^{fl/fl}$ mice and to assess MTA2/NuRD-regulated transcriptional programs in these cells, we performed RNA-sequencing (RNA-seq) analyses using pro-B cells and small pre-B cells from *Vav-Cre Mta2*$^{fl/fl}$ and control mice (the cell sorting strategies are like the ones shown in Figure S3B) (Figure 5A). Consistent with the observation that MTA2 enhances HDAC activity *in vitro*, as well as a general role of HDACs in gene repression (Feng and Zhang, 2003), many more genes were upregulated (440 genes >1.5-fold) than downregulated (88 genes >1.5-fold) in pro-B cells upon *Mta2* inactivation (Figure 5B). Among upregulated genes, about 8% (37) showed more than 3-fold increases in expression, while the rest (403) showed 1.5- to 3-fold increases in expression (Figure 5B). Among downregulated genes, about 6% (5) showed more than 3-fold reductions in expression, whereas 94% (83) showed 1.5- to 3-fold reductions (Figure 5B). A gene ontology (GO) analysis of upregulated genes in *Mta2*-deficient pro-B cells showed that the top enriched pathways or cellular processes include neutrophil degranulation and activation (e.g., *Cd14*, *Cd63*, *Chit1*, *Ckap4*, *Lrg1*, etc.); inflammatory responses (e.g., *Cebpb*, *Csf1r*, *Ptgir*, *Cd6*, *Cxcr2*, etc.); cell junction and extracellular matrix (ECM) relationships (e.g., *Tjp1*, *Prtn3*, *Itgb4*, *Col5a1*, etc.); macromolecule metabolism (e.g., *Acvrl1*, *ccr1*, and *Cd3e*, etc.); and endocytosis (e.g., *Cd63 Lrp1*, *Hip1*, *Apoe*, etc.) (Figure 5C). Other genes that showed more substantial (>3-fold) upregulation in Mta2-deficient pro-B cells include the following: *Gpr4*, *Asprv1*, *Rcn3*, *Ly6a*, *Padi3*, etc.

In the small pre-B cell compartment, there also were more genes upregulated (435 genes) than downregulated (229 genes) upon *Mta2* inactivation (>1.5-fold) (Figure 5B). Among upregulated genes, about 15% (62) showed more than 3-fold increases in expression, while the rest (373) showed 1.5- to 3-fold increases in expression (Figure 5B). Among downregulated genes, only 5% (12) showed more than 3-fold reductions in expression, whereas 95% showed 1.5- to 3-fold reductions (Figure 5B). A GO analysis showed that the top enriched pathways/cellular processes in *Mta2*-deficient pre-B cells include the following: T cell receptor (TCR) and T cell differentiation (e.g., *Lck*, *Thy1*, *Lat*, *Zap70*, etc.), regulation of apoptosis (e.g., *Bcl2*, *Ccnd2*, *Socs2*, *c-Kit*, etc.), and inositol phosphate metabolism (e.g., *Plcd3*, *Plcb3*, *Inpp4a*, etc.) (Figure 5C). Intriguingly, a group of genes involved in axon guidance (e.g., *Plxnd1*, *Plxnb2*, *Plxnc1*, etc.) are also repressed by MTA2 in pre-B cells (Figure 5C). A comparison of our RNA-seq data with previously reported gene profiling data revealed that genes normally silenced during BM B cell differentiation from Hardy Fr C′ (cycling pre-B) to Fr D (resting pre-B) stages (Ferreirós-Vidal et al., 2013) are enriched in upregulated genes in *Vav-Cre Mta2*$^{fl/fl}$ small pre-B cells (Figure S5A), indicating an important role of MTA2/NuRD at this development stage. Other MTA2-regulated genes that showed substantial upregulation (>3.5-fold) include the following: *Crhbp*, *Atp11a*, *Trim63*, *Ikzf2* (*Helios*), *Gprasp2*, *Rcn3*, *H1f0*, etc. Our RNA-seq data also confirmed increased expression of *Igll1* and *VpreB1* genes in small pre-B cells. Among MTA2-repressed genes in small pre-B cells, about 70% have MTA2 binding sites at loci of their human orthologs in 697 cells (Figure S5B), suggesting that these are potential direct MTA2 target genes in mouse pre-B cells. It is noteworthy that only 96 genes (21% of upregulated genes in *Mta2*-deficient pro-B cells, 22% of upregulated genes in *Mta2*-deficient small pre-B cells) are repressed by MTA2 in both pro-B cells and in pre-B cells (Figures 5C and S5C), suggesting that MTA2/NuRD regulates distinct transcriptional programs at different B cell developmental stages. The expression levels of a selected group of genes identified in *Mta2*-deficient pre-B cells by RNA-seq analyses have also been validated by RT-qPCR assays using cohorts of mice different from those used for RNA-seq analyses (Figure S5D).

Derepression of Pre-BCR Genes and a Pre-B to Immature B Transition Defect in Mice Lacking Both *Mta2* and *Oca-B* Genes

In addition to the fact that AIOLOS is a key transcription factor in repression of *Igll1* and *VpreB1* genes at the pre-B cell stage (Thompson et al., 2007), we previously found that the B cell-selective transcription coactivator OCA-B also represses *Igll1* and *VpreB1* genes at the pre-B stage through an interaction with SYK kinase in the cytoplasm (Siegel et al., 2006). Interestingly, the joint loss of AIOLOS and OCA-B caused a greater derepression of *Igll1* and *VpreB1* genes in pre-B cells than was observed in either of the single-KO mice, and also caused a more severe defect in the pre-B to immature B cell transition (Karnowski et al., 2008). To determine whether MTA2 also synergizes with OCA-B in a similar fashion, we generated *Vav-Cre Mta2* $^{fl/fl}$*; Oca-B*$^{-/-}$ mice (*DKO*) and examined BM B cell development in these mice. As shown in Figures 6A and 6B, the total number of BM cells in *DKO* mice decreased to one-third of the number in control mice, and both immature B and mature (recirculating) B cells showed 50% reductions. However, the population sizes of immature B and mature B cells showed 10-fold or more reductions, which are much more severe than those observed in either *Vav-Cre Mta2*$^{fl/fl}$ (Figures 2A and 2B) or *Oca-B*$^{-/-}$ (Figures 6A and 6B) mice. Like *Vav-Cre Mta2*$^{fl/fl}$ mice, the *DKO* mice also

(D) A heatmap generated by normalized read densities from individual ChIP-seq data (AIO, AIOLOS; IKA, IKAROS) centered at TSS and ranked by AIOLOS peak signals.

(E) Consensus AIOLOS-, IKAROS, MTA2, and HDAC2 recognition sequences identified by *de novo*-motif identification in 697 cells. The more detailed summaries of DNA motifs recognized by these factors are listed in Tables S1–S4.

(F) ChIP-seq snapshots of AIOLOS, IKAROS, HDAC2, and MTA2 binding at pre-BCR gene promoters in 697 cells. The scales of ChIP-seq signals are indicated.

A

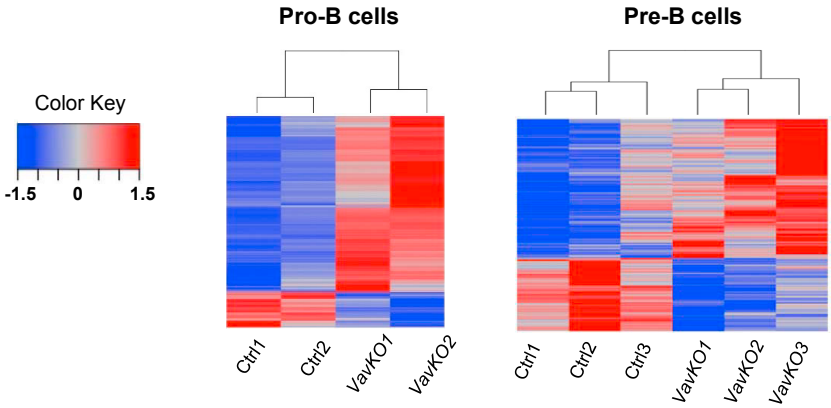

B

		up-regulation in KO (440 genes)			down-regulation in KO (88 genes)		
Pro-B cells	Fold change	>5	3 - 5	1.5-3	>5	3 - 5	1.5 - 3
	Number of genes	9	28	403	2	3	83

		up-regulation in KO (435 genes)			down-regulation in KO (229 genes)		
Pre-B cells	Fold change	>5	3 - 5	1.5-3	>5	3 - 5	1.5 - 3
	Number of genes	19	43	373	4	8	217

C

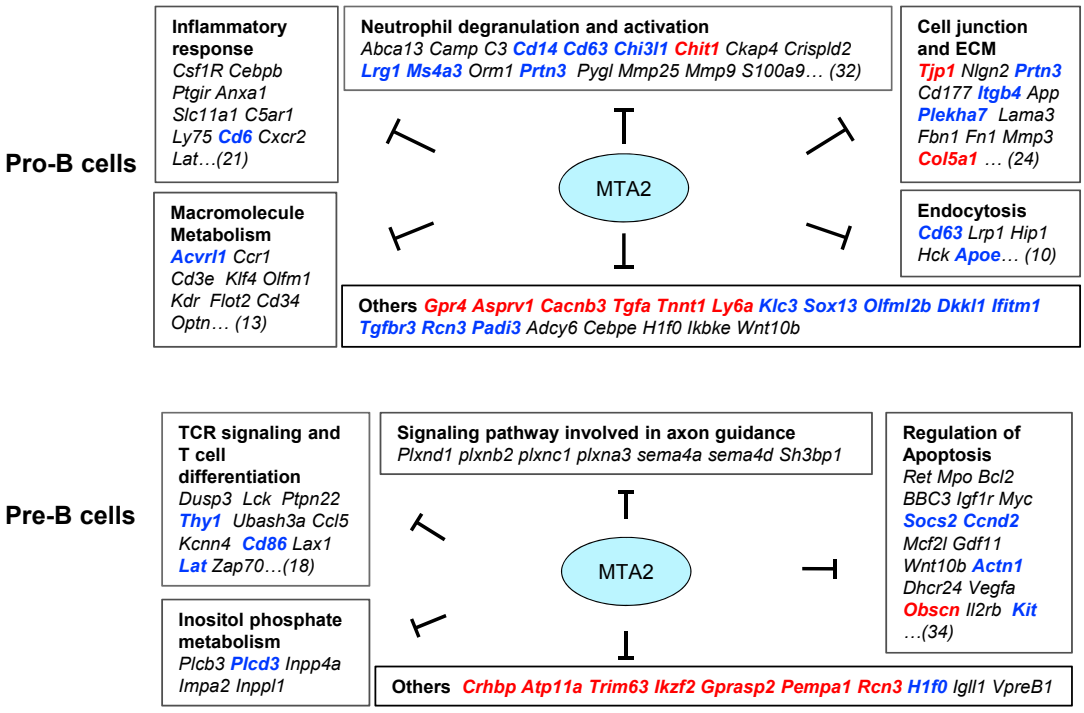

Figure 5. Distinct MTA2-Dependent Transcriptional Programs in Mouse Pro-B and Pre-B Cells

(A) Heatmaps based on RNA-seq data from *Vav-Cre Mta2*$^{fl/fl}$ (*VavKO*) and control pro-B (left) and small pre-B (right) cells.

(B) Numbers of genes that show increased or decreased expression in pro-B and small pre-B cells upon loss of *Mta2* (threshold 1.5-fold).

(C) Gene ontology (GO) analyses of MTA2-regulated pathways and processes in pro-B and small pre-B cells (black, 1.5- to 3-fold change; blue, 3-5-fold; red, >5-fold).

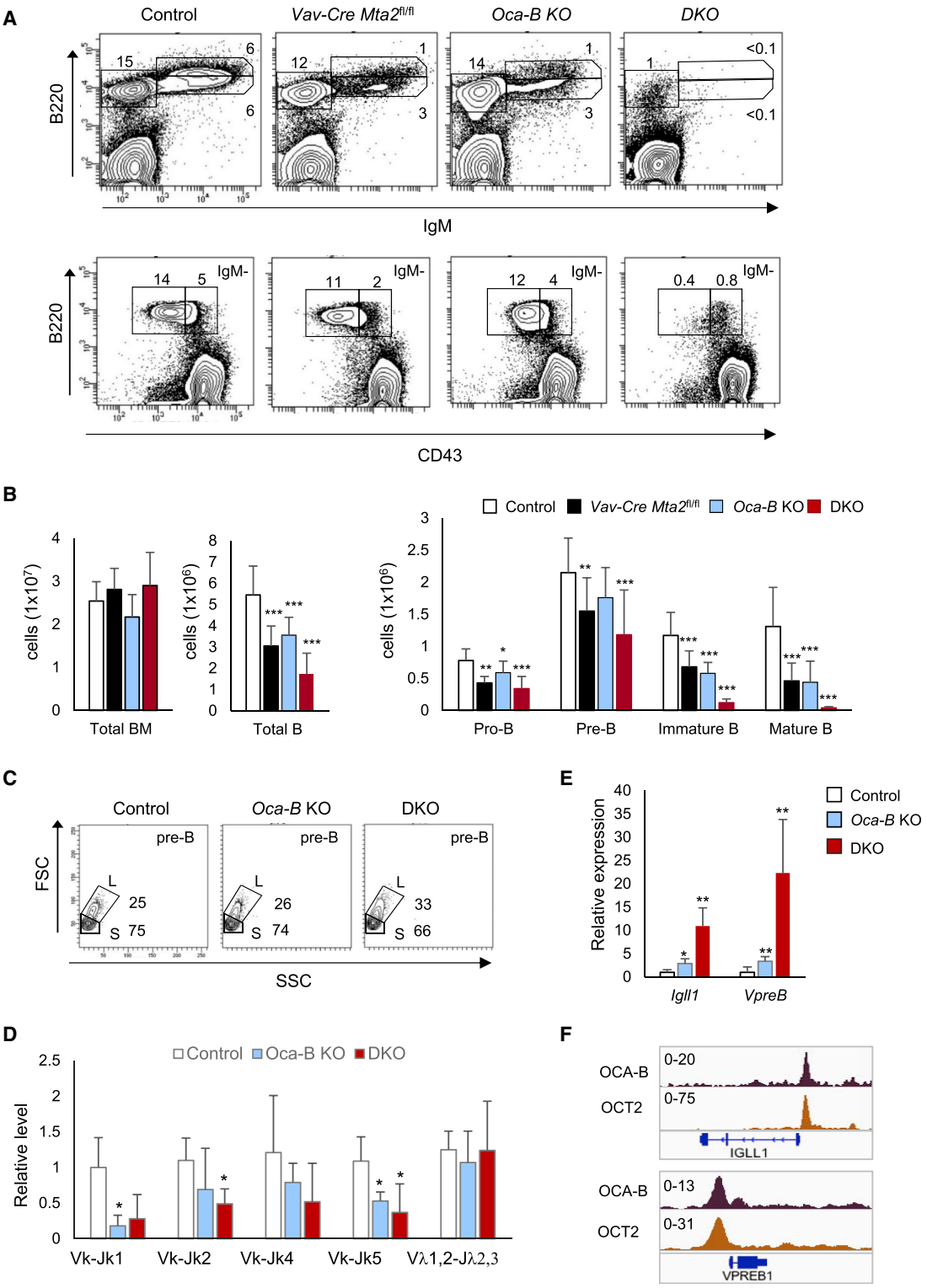

Figure 6. Joint Loss of MTA2 and OCA-B Causes Severe BM B Cell Developmental Defects

(A) Staining and gating of the of bone marrow B cell compartments in control, *Vav-Cre Mta2*$^{fl/fl}$, *Oca-B*$^{-/-}$, and *DKO* mice. Frequencies of indicated subpopulations are marked.

(B) Cell numbers of different B cell subsets (from two femurs) are plotted (n = 15 for control, n = 10 for *Oca-B*$^{-/-}$, and n = 7 for DKO mice; t test; *p < 0.05, ***p < 0.001).

(legend continued on next page)

showed an increased large pre-B to small pre-B cell ratio and abnormal Ig light chain κ rearrangements (Figures 6C and 6D).

We further examined the expression of *Igll1* and *VpreB1* genes in *Oca-B*$^{-/-}$ and *DKO* pre-B cells. While *Oca-B*$^{-/-}$ pre-B cells exhibited an approximate 3-fold increase of *Igll1* and *VpreB1* expression levels, the *DKO* pre-B cells show a 10- to 20-fold increase of *Igll1* and *VpreB1* expression (Figure 6E), demonstrating a synergy between OCA-B and MTA2/NuRD in *Igll1* and *VpreB1* repression at the pre-B stage. To further explore the possibility that OCA-B may directly regulate transcription of *Igll1* and *VpreB1*, ChIP and *OCA-B* knockdown experiments were carried out in 697 cells. As shown in Figures 6F and S6, the results not only demonstrate binding of both OCA-B and its interacting transcription factor OCT2 to *IGLL1* and *VPREB1* promoters but also confirm the *OCA-B*-mediated repression of *IGLL1* and *VPREB1* in pre-B cells—thus indicating a potential repression function of OCA-B.

The Role of MTA2 in the Differentiation and Function of Splenic B Cells

Unlike what is observed in *Mta2* Δ/Δ mice (Figure 1C), but similar to what is observed in *Cd19-Cre Mta2*$^{fl/fl}$ or *Mb1-Cre* Mta2$^{fl/fl}$ mice (Figure S2), *Vav-Cre Mta2*$^{fl/fl}$ mice show an increased MZB population that is about 2-fold the size of that in control mice (Figures 7A and 7E). The size of the FOB population is largely unaffected in these mice (Figures 7A and 7E). To assess the effect of MTA2 inactivation on the B cell response to immunization, we immunized *Vav-Cre Mta2*$^{fl/fl}$ and control mice with SRBCs (sheep red blood cells) for 9.5 days and then examined the differentiation of germinal center B (GC B) cells ($B220^{+}CD95^{+}CD38^{-}CD4^{-}$) in these mice. As shown in Figures 7B and 7C, *Mta2* inactivation leads to the production of more GC B cells during the immune response. *In vitro Ig* class switch assays also show abnormal class switching to *IgG1* and to *IgA* in the absence of MTA2 (Figure S7), suggesting an important role of MTA2/NuRD during an immune response.

Beyond a strong functional synergy between MTA2 and OCA-B in the pre-B to immature B transition, as shown in Figure 6, the dramatic loss of recirculating B cells in DKO mice also suggests a severe defect in splenic B cell development in these mice. A previous study has demonstrated a greater loss of splenic B cells in *Aiolos*$^{-/-}$, *Oca-B*$^{-/-}$ mice in comparison to either *Aiolos*$^{-/-}$ or *Oca-B*$^{-/-}$ mice (Sun et al., 2003). Similarly, while neither *Vav-Cre Mta2*$^{fl/fl}$ nor *Oca-B*$^{-/-}$ mice showed substantial loss of FOB cells, and only *Oca-B*$^{-/-}$ but not *Vav-Cre Mta2*$^{fl/fl}$ mice showed a decrease in the MZB cell population (Figures 7D and 7E), the *DKO* mice exhibited dramatic decreases in both FOB and MZB populations—thus demonstrating an MTA2 and/or OCA-B requirement for the development of splenic B cell compartments (Figures 7D and 7E). These data further support our hypothesis that AIOLOS functions in peripheral B cells through its interaction with MTA2/NuRD.

DISCUSSION

Despite intensive studies of key transcription factors involved in B cell lineage specification and development, less is clear about the roles of transcription cofactors such as chromatin regulators during this process. Here, through a combination of genetic, biochemical, and genomic approaches, we directly assessed the contributions of NuRD corepressor complexes to BM and splenic B cell development.

Our data demonstrate that MTA2/NuRD plays an important role at multiple stages during B cell development in BM and spleen. Initially, we found decreased BM B cell subsets (pro-B, pre-B, and immature B populations) and MZB cells in *Mta2* Δ/Δ mice. Surprisingly, neither *Cd19*-Cre *Mta2*$^{fl/fl}$ nor *Mb1*-Cre *Mta2*$^{fl/fl}$ mice recapitulated the BM defects observed in *Mta2* Δ/Δ mice. The incomplete deletion efficiencies observed in *Cd19*-Cre *Mta2*$^{fl/fl}$ and *Mb1*-Cre *Mta2*$^{fl/fl}$ pro-B cells are likely an important factor for causing this phenomenon. In contrast, *Vav*-Cre *Mta2*$^{fl/fl}$ mice exhibit optimal deletion efficiency in pro-B, pre-B, and immature B cells and recapitulate the BM B cell development defects of *Mta2* Δ/Δ mice. We also show that *Mta2* inactivation causes abnormal rearrangements of Ig heavy chain genes in pro-B cells. In relation to Ig light chain rearrangements in pre-B cells, our data suggest a greater effect of *Mta2* inactivation on more distal events relative to proximal events, likely a result of premature termination of recombination processes. Loss of MTA2 also leads to an increased large pre-B to small pre-B ratio and a decrease in the small pre-B population, suggesting a cell cycle defect at the pre-B stage and a likely effect on the pre-B to immature B cell transition. In the spleen, where *Mta2* Δ/Δ mice show an approximate 5-fold reduction of MZB cells, the *Cd19*-Cre *Mta2*$^{fl/fl}$, *Mb1*-Cre *Mta2*$^{fl/fl}$, and *Vav*-Cre *Mta2*$^{fl/fl}$ mice show, instead, an approximately 2-fold increase in MZB cells. These results suggest a potential B cell-extrinsic role for MTA2 (e.g., in stromal cells) in regulating MZB population size in *Mta2* Δ/Δ mice.

At the molecular level, gene profiling analyses have identified genes suppressed by MTA2 in pro-B cells and small pre-B cells (non-dividing pre-B cells). GO analyses indicate that MTA2/NuRD regulates distinct transcriptional programs in pro-B and pre-B cells. In pro-B cells, the major pathways suppressed by MTA2/NuRD include neutrophil degranulation and activation, cell junction and ECM, inflammation response, macromolecule metabolism, and endocytosis (Figure 5C). In pre-B cells, the major pathways repressed by MTA2/NuRD include TCR signaling and T cell differentiation, regulation of apoptosis, and axon guidance (Figure 5C). It thus appears that MTA2/NuRD is involved in the repression of non-B lineage genes at both pro-B and pre-B stages. Furthermore, a gene set enrichment analysis (GSEA) indicates that genes normally silenced during Hardy Fr C′ (cycling pre-B) to Hardy Fr D (resting pre-B) differentiation are enriched in upregulated genes in *Mta2*-deficient small pre-B cells.

(C) Representative FACS data showing frequencies of large pre-B (L) and small pre-B (S) cells in mice with indicated genotypes.
(D) Real-time PCR results indicating relative abundances of different Ig light chain VJ rearrangements in small pre-B cells isolated from mice with indicated genotypes (n = 4 for each genotype; t test, *p < 0.05).
(E) RT-qPCR results showing increased *Igll1* and *VpreB1* expression levels in *Oca-B*$^{-/-}$ and *DKO* pre-B cells (n ≥ 3 for each genotype; t test; *p < 0.05, **p < 0.01).
(F) ChIP-seq snapshots of OCA-B and OCT2 binding at *IGLL1* and *VPREB1* promoter regions in 697 cells. The scales of ChIP-seq signals are indicated.

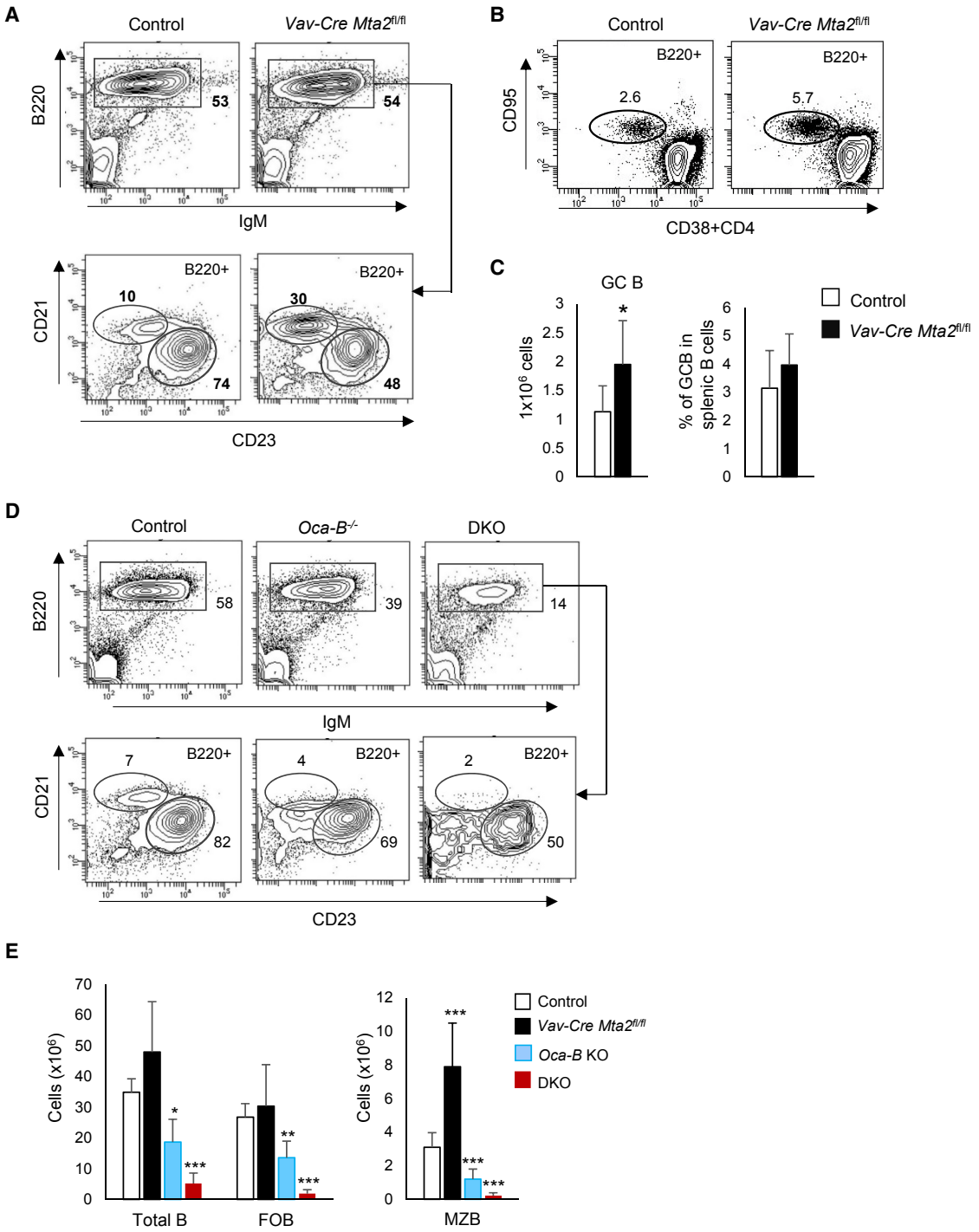

Figure 7. Abnormal Splenic B Cell Differentiation and B Cell Response in Mice Lacking MTA2 or Both MTA2 and OCA-B

(A) Staining of total splenic B ($B220^+$), marginal zone B (MZB) ($B220^+CD21^{hi}CD23^{lo}$), and follicular B (FOB) ($B220^+CD21^-CD23^{hi}$) cells in *Vav-Cre Mta2*$^{fl/fl}$ and control mice. Frequencies of different cell populations in parental cells are indicated.

(B) Staining of germinal center B (GCB) ($B220^+CD95^+CD38^-CD4^-$) cells in *Vav-Cre Mta2*$^{fl/fl}$ and control mice immunized by sheep red blood cells (SRBCs).

(C) Numbers of GCB cells and frequencies of GCB cells in splenic B cells are plotted (n = 8 for each genotype; t test; *p = 0.02).

(D) Staining of splenic B, MZB, and FOB cells in mice with indicated genotypes.

(E) Cell numbers of different B cell subsets are plotted (n = 10 for control, n = 9 for *Vav-Cre Mta2*$^{fl/fl}$, n = 5 for *Oca-B*$^{-/-}$ and DKO mice; t test; *p < 0.05, **p < 0.01, ***p < 0.001).

It is worth noting that, although other MTA family member genes, namely *Mta3* and *Mta1*, are also expressed in different B subsets cells, our data demonstrate non-redundant functions of MTA2 during B cell development. Further analyses are required to elucidate the unique function of MTA1 and MTA3 and redundant function between MTA family members during B cell development.

The B cell phenotypes described above and other defects of immune system caused by loss of MTA2 function are strikingly similar to those associated with loss of AIOLOS function (Table S5; Karnowski et al., 2008; Lu et al., 2008; Sun et al., 2003; Wang et al., 1998). Consistent with previous observations of an IKAROS/AIOLOS/NuRD association in T cells (Kim et al., 1999; Zhang et al., 2011), we have shown a physical interaction between AIOLOS/IKAROS and MTA2/NuRD in B cells. This observation opened a window into the functional interplay between AIOLOS/IKAROS and MTA2/NuRD complexes. Specifically, it was already noted that *Igll1* and *VpreB1*, two genes central to the pre-B cell differentiation, are derepressed in *Aiolos*$^{-/-}$ pre-B cells (Thompson et al., 2007). Conversely, overexpression of IKAROS in B3 mouse pre-B cells recruits MI-2β and MBD3 to its binding sites and causes rapid RNA polymerase II eviction, reduced promoter accessibility, and repression of Ikaros-bound genes that include *Igll1* and *VpreB1* in a MI-2β-dependent manner (Ferreirós-Vidal et al., 2013; Liang et al., 2017). In this study, our data from RT-qPCR, ChIP-qPCR, and ChIP-seq analyses all strongly support a model in which AIOLOS/IKAROS represses pre-BCR gene expression through an interaction with MTA2/NuRD.

Beyond pre-BCR gene loci, genome-wide mapping of AIOLOS, IKAROS, HDAC2, and MTA2 binding sites in human 697 cells showed a highly significant overlap between AIOLOS/IKAROS targets and NuRD targets (Figures 4C and 4D). Motif analyses showed that EBF1, RUNX1/2, and ETS family binding sites are among the top motifs enriched in DNA sequences bound by AIOLOS, IKAROS, HDAC2, and MTA2. Integration of ChIP-seq data with gene profiling data showed that the human orthologs of about 70% of the upregulated genes in *Vav-Cre Mta2*$^{fl/fl}$ pre-B cells are direct MTA2 targets in human pre-B cells. These data support the hypothesis that transcriptional repression through NuRD and transcription repressors (such as AIOLOS/IKAROS) might be achieved, at least in part, by competition with transcription activators (such as EBF1) and associated coactivators (such as p300/CBP) at promoters or enhancer elements.

At the periphery, while both *Mta2* Δ/Δ and *Aiolos*-null mice show loss of MZB cells, the *Mta2* B cell-specific null mice (*Cd19-Cre*-, *Mb1-Cre*, and *Vav-Cre Mta2*$^{fl/fl}$) show an increase of MZB cells, implying a possible stromal cell-related MTA2 function that affects the MZB population size. It will be interesting to determine whether the B cell-specific inactivation of *Aiolos* leads to a similar phenotype. Consistent with the B cell activation phenotype in *Aiolos*-null mice, we observed increased GC B cell production in response to SRBC stimulation in *Vav-Cre Mta2*$^{fl/fl}$ mice. It is worth noting that B cell-specific *Ikaros* KO mice also show dramatic losses of pre-B, immature B, and recirculating B in bone marrow, and both MZB and FOB cells in spleen, but increased splenic B1-B cells (Macias-Garcia et al., 2016; Schwickert et al., 2014)—demonstrating non-redundant functions of different IKAROS family members during B cell development.

OCA-B is a transcription coactivator that plays an essential role in GC formation and transcription of secondary Ig genes, and that is also involved in B cell development in the bone marrow (Luo and Roeder, 1999; Siegel et al., 2006). Our previous study had shown that OCA-B represses pre-BCR genes *Igll1* and *VpreB1* in pre-B cells, likely through its interaction with SYK kinase in the cytoplasm (Siegel et al., 2006). However, the current ChIP data demonstrate a direct binding of OCA-B and its interacting transcription factor OCT2 at *IGLL1* and *VPREB1* promoters in 697 cells. Moreover, *OCA-B* knockdown in 697 cells reproduces the derepression of *Igll1* and *VpreB1* genes. Notably, these results indicate an important and previously unrecognized repressive function of OCA-B at these gene loci. Similar to what was observed in *Aiolos*$^{-/-}$; *Oca-B*$^{-/-}$ mice (Karnowski et al., 2008), we observed a substantial increase in *Igll1* and *VpreB1* expression in *Vav-Cre Mta2*$^{fl/fl}$; *Oca-B*$^{-/-}$ pre-B cells, along with a severe developmental block in the pre-B to immature B transition and a significant loss of MZB and FOB cells in the spleen. These data further support our model in which AIOLOS depends on MTA2/NuRD to execute its function both in BM pre-B cells and in peripheral B cells. This synergy is significant since several previous studies exploring genetic interactions of OCA-B with OCT2, NFκB, and BTK did not show severe BM B cell developmental defects in respective double-mutant mice (Kim et al., 2000; Schubart et al., 2000, 2001). The increased MZB cells in *Vav-Cre Mta2*$^{fl/fl}$ mice and the dramatic losses of MZB cells in both *Oca-B*$^{-/-}$ and DKO mice suggest that OCA-B functions downstream of MTA2/NuRD in regulating MZB cell differentiation.

In summary, our analysis of *Mta2*-deficient mice demonstrates an important role of the MTA2/NuRD complex in B cell development. The phenotypic similarity, physical interaction, and overlapping genome-wide binding sites between MTA2 and AIOLOS/IKAROS present a striking example in which inactivation of a transcription cofactor (MTA2) recapitulates the defects caused by inactivation of a transcription factor (AIOLOS) *in vivo*, strongly suggesting a mutual functional dependence between MTA2/NuRD and AIOLOS/IKAROS during B cell development. Our data have also demonstrated a strong genetic interaction between MTA2/NuRD and OCA-B in regulating *Igll1* and *VpreB1* expression and the pre-B to immature B cell transition. The *Vav-Cre Mta2*$^{fl/fl}$; *Oca-B*$^{-/-}$ model could serve as a platform for future elucidation of key pathways controlling the pre-B to immature B cell checkpoint and peripheral B cell development.

STAR★METHODS

Detailed methods are provided in the online version of this paper and include the following:

- KEY RESOURCES TABLE
- LEAD CONTACT AND MATERIALS AVAILABILITY
- EXPERIMENTAL MODEL AND SUBJECT DETAILS
  - Mice
  - Cell Line
- METHOD DETAILS
  - Flow Cytometry
  - Immunoprecipitation (IP)
  - RNA isolation and reverse transcription (RT)

- Quantitative PCR
- RNA-seq and gene ontology
- Genomic rearrangement of the Immunoglobulin heavy chain and light chain loci
- Chromatin immunoprecipitation (ChIP) and ChIP-sequencing
- Data analysis for ChIP-seq
- shRNA knockdown
- Immunization and immunoglobulin (Ig) class switch

- QUANTIFICATION AND STATISTICAL ANALYSIS
- DATA AND CODE AVAILABILITY

SUPPLEMENTAL INFORMATION

Supplemental Information can be found online at https://doi.org/10.1016/j.celrep.2019.06.029.

ACKNOWLEDGMENTS

We thank Alexander Tarakhovsky, and Joon Seok Park at The Rockefeller University, Hongsheng Wang at NIH, Ivan Maillard at University of Michigan, and Zhixin Zhang at University of Nebraska Medical Center for valuable comments and suggestions. We thank the Rockefeller University Flow Cytometry Resource Center and UNC-Chapel Hill Flow Cytometry Center for cell sorting and other technical help, and the Rockefeller University Genomics Core Facility for sequencing analysis. This work was supported by grant CA178765 to R.G.R. from NIH, United States. X.L. was supported in part by grant UL1 TR000043 from the National Center for Advancing Translational Sciences, NIH, United States and co-sponsored by the Shapiro-Silverberg Fund for the Advancement of Translational Research, United States.

AUTHOR CONTRIBUTIONS

X.L., C.-S.C., T.F., V.R.-E., A.P., and Y.Q. did the experiments. F.F. and C.-S.C. performed bioinformatics analysis. S.H.C., Y.Z., A.M.M., and F.N.P. provided advice, reagents, and support. X.L., F.N.P., and R.G.R. designed the experiments and wrote the manuscript.

DECLARATION OF INTERESTS

The authors declare no competing interests.

Received: March 1, 2018
Revised: April 21, 2019
Accepted: June 6, 2019
Published: July 9, 2019

REFERENCES

Avitahl, N., Winandy, S., Friedrich, C., Jones, B., Ge, Y., and Georgopoulos, K. (1999). Ikaros sets thresholds for T cell activation and regulates chromosome propagation. Immunity *10*, 333–343.

Bagheri-Yarmand, R., Balasenthil, S., Gururaj, A.E., Talukder, A.H., Wang, Y.H., Lee, J.H., Kim, Y.S., Zhang, X., Jones, D.M., Medeiros, L.J., et al. (2007). Metastasis-associated protein 1 transgenic mice: a new model of spontaneous B-cell lymphomas. Cancer Res. *67*, 7062–7067.

Busslinger, M. (2004). Transcriptional control of early B cell development. Annu. Rev. Immunol. *22*, 55–79.

Busslinger, M., and Tarakhovsky, A. (2014). Epigenetic control of immunity. Cold Spring Harb. Perspect. Biol. *6*, a019307.

Dege, C., and Hagman, J. (2014). Mi-2/NuRD chromatin remodeling complexes regulate B and T-lymphocyte development and function. Immunol. Rev. *261*, 126–140.

Denslow, S.A., and Wade, P.A. (2007). The human Mi-2/NuRD complex and gene regulation. Oncogene *26*, 5433–5438.

Feng, Q., and Zhang, Y. (2003). The NuRD complex: linking histone modification to nucleosome remodeling. Curr. Top. Microbiol. Immunol. *274*, 269–290.

Ferreirós-Vidal, I., Carroll, T., Taylor, B., Terry, A., Liang, Z., Bruno, L., Dharmalingam, G., Khadayate, S., Cobb, B.S., Smale, S.T., et al. (2013). Genome-wide identification of Ikaros targets elucidates its contribution to mouse B-cell lineage specification and pre-B-cell differentiation. Blood *121*, 1769–1782.

Fujita, N., Jaye, D.L., Geigerman, C., Akyildiz, A., Mooney, M.R., Boss, J.M., and Wade, P.A. (2004). MTA3 and the Mi-2/NuRD complex regulate cell fate during B lymphocyte differentiation. Cell *119*, 75–86.

Gao, H., Lukin, K., Ramírez, J., Fields, S., Lopez, D., and Hagman, J. (2009). Opposing effects of SWI/SNF and Mi-2/NuRD chromatin remodeling complexes on epigenetic reprogramming by EBF and Pax5. Proc. Natl. Acad. Sci. USA *106*, 11258–11263.

Heinz, S., Benner, C., Spann, N., Bertolino, E., Lin, Y.C., Laslo, P., Cheng, J.X., Murre, C., Singh, H., and Glass, C.K. (2010). Simple combinations of lineage-determining transcription factors prime *cis*-regulatory elements required for macrophage and B cell identities. Mol. Cell *38*, 576–589.

Hobeika, E., Thiemann, S., Storch, B., Jumaa, H., Nielsen, P.J., Pelanda, R., and Reth, M. (2006). Testing gene function early in the B cell lineage in mb1-cre mice. Proc. Natl. Acad. Sci. USA *103*, 13789–13794.

Kamps, M.P., Look, A.T., and Baltimore, D. (1991). The human t(1;19) translocation in pre-B ALL produces multiple nuclear E2A-Pbx1 fusion proteins with differing transforming potentials. Genes Dev. *5*, 358–368.

Karnowski, A., Cao, C., Matthias, G., Carotta, S., Corcoran, L.M., Martensson, I.L., Skok, J.A., and Matthias, P. (2008). Silencing and nuclear repositioning of the lambda5 gene locus at the pre-B cell stage requires Aiolos and OBF-1. PLoS ONE *3*, e3568.

Kim, U., Qin, X.F., Gong, S., Stevens, S., Luo, Y., Nussenzweig, M., and Roeder, R.G. (1996). The B-cell-specific transcription coactivator OCA-B/OBF-1/Bob-1 is essential for normal production of immunoglobulin isotypes. Nature *383*, 542–547.

Kim, J., Sif, S., Jones, B., Jackson, A., Koipally, J., Heller, E., Winandy, S., Viel, A., Sawyer, A., Ikeda, T., et al. (1999). Ikaros DNA-binding proteins direct formation of chromatin remodeling complexes in lymphocytes. Immunity *10*, 345–355.

Kim, U., Gunther, C.S., and Roeder, R.G. (2000). Genetic analyses of NFKB1 and OCA-B function: defects in B cells, serum IgM level, and antibody responses in Nfkb1−/−Oca-b−/− mice. J. Immunol. *165*, 6825–6832.

Kim, D., Pertea, G., Trapnell, C., Pimentel, H., Kelley, R., and Salzberg, S.L. (2013). TopHat2: accurate alignment of transcriptomes in the presence of insertions, deletions and gene fusions. Genome Biol. *14*, R36.

Kim, J.Y., Kwak, P.B., and Weitz, C.J. (2014). Specificity in circadian clock feedback from targeted reconstitution of the NuRD corepressor. Mol. Cell *56*, 738–748.

Krop, I., de Fougerolles, A.R., Hardy, R.R., Allison, M., Schlissel, M.S., and Fearon, D.T. (1996). Self-renewal of B-1 lymphocytes is dependent on CD19. Eur. J. Immunol. *26*, 238–242.

Kühn, R., Schwenk, F., Aguet, M., and Rajewsky, K. (1995). Inducible gene targeting in mice. Science *269*, 1427–1429.

Kuleshov, M.V., Jones, M.R., Rouillard, A.D., Fernandez, N.F., Duan, Q., Wang, Z., Koplev, S., Jenkins, S.L., Jagodnik, K.M., Lachmann, A., et al. (2016). Enrichr: a comprehensive gene set enrichment analysis web server 2016 update. Nucleic Acids Res. *44* (*W1*), W90–W97.

Langmead, B., and Salzberg, S.L. (2012). Fast gapped-read alignment with Bowtie 2. Nat. Methods *9*, 357–359.

Li, H., Handsaker, B., Wysoker, A., Fennell, T., Ruan, J., Homer, N., Marth, G., Abecasis, G., and Durbin, R.; 1000 Genome Project Data Processing Subgroup (2009). The sequence alignment/map format and SAMtools. Bioinformatics *25*, 2078–2079.

Liang, Z., Brown, K.E., Carroll, T., Taylor, B., Vidal, I.F., Hendrich, B., Rueda, D., Fisher, A.G., and Merkenschlager, M. (2017). A high-resolution map of transcriptional repression. eLife *6*, e22767.

Loughran, S.J., Comoglio, F., Hamey, F.K., Giustacchini, A., Errami, Y., Earp, E., Göttgens, B., Jacobsen, S.E.W., Mead, A.J., Hendrich, B., and Green, A.R. (2017). Mbd3/NuRD controls lymphoid cell fate and inhibits tumorigenesis by repressing a B cell transcriptional program. J. Exp. Med. *214*, 3085–3104.

Lu, X., Kovalev, G.I., Chang, H., Kallin, E., Knudsen, G., Xia, L., Mishra, N., Ruiz, P., Li, E., Su, L., and Zhang, Y. (2008). Inactivation of NuRD component Mta2 causes abnormal T cell activation and lupus-like autoimmune disease in mice. J. Biol. Chem. *283*, 13825–13833.

Luo, Y., and Roeder, R.G. (1999). B-cell-specific coactivator OCA-B: biochemical aspects, role in B-cell development and beyond. Cold Spring Harb. Symp. Quant. Biol. *64*, 119–131.

Macias-Garcia, A., Heizmann, B., Sellars, M., Marchal, P., Dali, H., Pasquali, J.L., Muller, S., Kastner, P., and Chan, S. (2016). Ikaros is a negative regulator of B1 cell development and function. J. Biol. Chem. *291*, 9073–9086.

Matthias, P., and Rolink, A.G. (2005). Transcriptional networks in developing and mature B cells. Nat. Rev. Immunol. *5*, 497–508.

Ogilvy, S., Metcalf, D., Gibson, L., Bath, M.L., Harris, A.W., and Adams, J.M. (1999). Promoter elements of vav drive transgene expression in vivo throughout the hematopoietic compartment. Blood *94*, 1855–1863.

Rickert, R.C., Roes, J., and Rajewsky, K. (1997). B lymphocyte-specific, Cre-mediated mutagenesis in mice. Nucleic Acids Res. *25*, 1317–1318.

Robinson, M.D., McCarthy, D.J., and Smyth, G.K. (2010). edgeR: a Bioconductor package for differential expression analysis of digital gene expression data. Bioinformatics *26*, 139–140.

Robinson, J.T., Thorvaldsdóttir, H., Winckler, W., Guttman, M., Lander, E.S., Getz, G., and Mesirov, J.P. (2011). Integrative genomics viewer. Nat. Biotechnol. *29*, 24–26.

Schubart, D.B., Rolink, A., Schubart, K., and Matthias, P. (2000). Cutting edge: lack of peripheral B cells and severe agammaglobulinemia in mice simultaneously lacking Bruton's tyrosine kinase and the B cell-specific transcriptional coactivator OBF-1. J. Immunol. *164*, 18–22.

Schubart, K., Massa, S., Schubart, D., Corcoran, L.M., Rolink, A.G., and Matthias, P. (2001). B cell development and immunoglobulin gene transcription in the absence of Oct-2 and OBF-1. Nat. Immunol. *2*, 69–74.

Schwickert, T.A., Tagoh, H., Gültekin, S., Dakic, A., Axelsson, E., Minnich, M., Ebert, A., Werner, B., Roth, M., Cimmino, L., et al. (2014). Stage-specific control of early B cell development by the transcription factor Ikaros. Nat. Immunol. *15*, 283–293.

Sen, N., Gui, B., and Kumar, R. (2014). Physiological functions of MTA family of proteins. Cancer Metastasis Rev. *33*, 869–877.

Shen, L., Shao, N., Liu, X., and Nestler, E. (2014). ngs.plot: quick mining and visualization of next-generation sequencing data by integrating genomic databases. BMC Genomics *15*, 284.

Siegel, R., Kim, U., Patke, A., Yu, X., Ren, X., Tarakhovsky, A., and Roeder, R.G. (2006). Nontranscriptional regulation of SYK by the coactivator OCA-B is required at multiple stages of B cell development. Cell *125*, 761–774.

Subramanian, A., Tamayo, P., Mootha, V.K., Mukherjee, S., Ebert, B.L., Gillette, M.A., Paulovich, A., Pomeroy, S.L., Golub, T.R., Lander, E.S., and Mesirov, J.P. (2005). Gene set enrichment analysis: a knowledge-based approach for interpreting genome-wide expression profiles. Proc. Natl. Acad. Sci. USA *102*, 15545–15550.

Sun, J., Matthias, G., Mihatsch, M.J., Georgopoulos, K., and Matthias, P. (2003). Lack of the transcriptional coactivator OBF-1 prevents the development of systemic lupus erythematosus-like phenotypes in Aiolos mutant mice. J. Immunol. *170*, 1699–1706.

Teitell, M.A. (2003). OCA-B regulation of B-cell development and function. Trends Immunol. *24*, 546–553.

Thompson, E.C., Cobb, B.S., Sabbattini, P., Meixlsperger, S., Parelho, V., Liberg, D., Taylor, B., Dillon, N., Georgopoulos, K., Jumaa, H., et al. (2007). Ikaros DNA-binding proteins as integral components of B cell developmental-stage-specific regulatory circuits. Immunity *26*, 335–344.

Trapnell, C., Williams, B.A., Pertea, G., Mortazavi, A., Kwan, G., van Baren, M.J., Salzberg, S.L., Wold, B.J., and Pachter, L. (2010). Transcript assembly and quantification by RNA-seq reveals unannotated transcripts and isoform switching during cell differentiation. Nat. Biotechnol. *28*, 511–515.

Wang, J.H., Avitahl, N., Cariappa, A., Friedrich, C., Ikeda, T., Renold, A., Andrikopoulos, K., Liang, L., Pillai, S., Morgan, B.A., and Georgopoulos, K. (1998). Aiolos regulates B cell activation and maturation to effector state. Immunity *9*, 543–553.

Williams, C.J., Naito, T., Arco, P.G., Seavitt, J.R., Cashman, S.M., De Souza, B., Qi, X., Keables, P., Von Andrian, U.H., and Georgopoulos, K. (2004). The chromatin remodeler Mi-2beta is required for CD4 expression and T cell development. Immunity *20*, 719–733.

Yamada, T., Yang, Y., Hemberg, M., Yoshida, T., Cho, H.Y., Murphy, J.P., Fioravante, D., Regehr, W.G., Gygi, S.P., Georgopoulos, K., and Bonni, A. (2014). Promoter decommissioning by the NuRD chromatin remodeling complex triggers synaptic connectivity in the mammalian brain. Neuron *83*, 122–134.

Yang, Y., Yamada, T., Hill, K.K., Hemberg, M., Reddy, N.C., Cho, H.Y., Guthrie, A.N., Oldenborg, A., Heiney, S.A., Ohmae, S., et al. (2016). Chromatin remodeling inactivates activity genes and regulates neural coding. Science *353*, 300–305.

Yoshida, T., Hazan, I., Zhang, J., Ng, S.Y., Naito, T., Snippert, H.J., Heller, E.J., Qi, X., Lawton, L.N., Williams, C.J., and Georgopoulos, K. (2008). The role of the chromatin remodeler Mi-2beta in hematopoietic stem cell self-renewal and multilineage differentiation. Genes Dev. *22*, 1174–1189.

Yu, M., Yang, W., Ni, T., Tang, Z., Nakadai, T., Zhu, J., and Roeder, R.G. (2015). RNA polymerase II-associated factor 1 regulates the release and phosphorylation of paused RNA polymerase II. Science *350*, 1383–1386.

Zhang, J., Jackson, A.F., Naito, T., Dose, M., Seavitt, J., Liu, F., Heller, E.J., Kashiwagi, M., Yoshida, T., Gounari, F., et al. (2011). Harnessing of the nucleosome-remodeling-deacetylase complex controls lymphocyte development and prevents leukemogenesis. Nat. Immunol. *13*, 86–94.

STAR★METHODS

KEY RESOURCES TABLE

REAGENT or RESOURCE	SOURCE	IDENTIFIER
Antibodies		
PE/Cy7 anti-mouse/human CD45R/B220	BioLegend	Cat# 103222; RRID: AB_313005
PE anti-mouse IgM	BioLegend	Cat# 406508; RRID: AB_315058
APC anti-mouse IgM	BioLegend	Cat# 406509; RRID: AB_315059
FITC anti-mouse CD43	BioLegend	Cat# 143204; RRID: AB_10960745
FITC anti-mouse CD21/CD35 (CR2/CR1)	BioLegend	Cat# 123407; RRID: AB_940403
PE anti-mouse CD23	BioLegend	Cat# 101607; RRID: AB_312832
Biotin anti-mouse Ly-51 (6C3/BP-1)	BioLegend	Cat# 108303; RRID: AB_313360
PE Streptavidin	BioLegend	Cat# 405203; RRID: N/A
APC anti-mouse CD24 (HAS)	BioLegend	Cat# 138505; RRID: AB_2565650
Brilliant Violet 605 anti-mouse IgM	BioLegend	Cat# 406523; RRID: AB_2563358
PerCP/Cyanine5.5 anti-mouse CD95(Fas)	BioLegend	Cat# 152610; RRID: AB_2632905
APC anti-mouse CD38	BioLegend	Cat# 102712; RRID: AB_312933
APC anti-mouse CD4	BioLegend	Cat# 116014; RRID: AB_2563025
PE anti-mouse IgG1	BioLegend	Cat# 406607; RRID: AB_10551439
Biotin anti-mouse IgG3	BioLegend	Cat# 406803; RRID: AB_315070
Biotin anti-mouse IgA	BioLegend	Cat# 407003; RRID: AB_315078
Anti-mouse CD40	BioLegend	Cat# 102802; RRID: AB_312935
Anti-Mta2	Abcam	Cat# ab8106; RRID: AB_306276
Anti-CHD4 (Mi-2β)	Abcam	Cat# ab72418; RRID: AB_1268107
Anti-IKZF3 (Aiolos)	Abcam	Cat# ab139408; RRID: N/A
Anti-IKZF1 (Ikaros)	Abcam	Cat# ab 26083; RRID: AB_881148
Anti-Bob1 (Oca-B) (C-20)	Santa Cruz Biotechnology	Cat# sc-955; RRID: AB_2166917
Anti-Oct-2 (C-20)	Santa Cruz Biotechnology	Cat# sc-233; RRID: AB_2167205
Anti-HDAC2	Abcam	Cat# ab7029; RRID: AB_305706
Anti-Histone H3 (tri methyl K4)	Abcam	Cat# ab8580; RRID: AB_306649
Anti-Histone H3 (acetyl K27)	Abcam	Cat# ab4729; RRID: AB_2118291
Anti-Histone H3	Abcam	Cat# ab1791; RRID: AB_302613
Normal rabbit IgG	Santa Cruz Biotechnology	Cat# sc-2027; RRID: AB_737197
Chemicals, Peptides, and Recombinant Proteins		
DSG (disuccinimidyl glutarate)	Thermo Fisher Scientific	Cat# 20593
Recombinant Murine IL-4	PeproTech	Cat# 214-14
Recombinant TGF-β (carrier free)	BioLegend	Cat# 763102
Critical Commercial Assays		
Arcturus™ PicoPure RNA isolation Kit	Applied Biosystems	Cat# KIT0204
qScript cDNA SuperMix	Quanta Biosciences	Cat# 95048
DNeasy Blood and Tissue Kit	QIAGEN	Cat# 69506
QuantiTect SYBR Green PCR mix	QIAGEN	Cat# 204145
JumpStart TaqReady Mix	Sigma-Aldrich	Cat# P2893
End-It™ End-Repair Kit	Epicenter	Cat# ER81050
DNA Clean & Concentrator Kit	Zymo Research	Cat# D4014
NEXTflexChIP-Seq Barcodes	PerkinElmer	Cat# NOVA-514120
Dynabeads™ Protein G	Invitrogen	Cat# 10004D
TruSeq Stranded mRNA Library Prep Kit	Illumina	Cat# 20020594
Mouse CD43 MicroBeads	Miltenyi Biotec	Cat# 130-049-801

(*Continued on next page*)

Continued

REAGENT or RESOURCE	SOURCE	IDENTIFIER
Deposited Data		
Mta2 Control_(781t4)_pro-B	This Paper	GSM3398870
Mta2 Control_(789t7)_pro-B	This Paper	GSM3398871
Vav-Cre Mta2 $^{f/f}$ _(781t3)_pro-B	This Paper	GSM3398872
Vav-Cre Mta2 $^{f/f}$ _(789t6)_pro-B	This Paper	GSM3398873
Mta2 Control_(918t3)_pre-B	This Paper	GSM3398874
Mta2 Control_(919t7)_pre-B	This Paper	GSM3398875
Mta2 Control _(931t10)_pre-B	This Paper	GSM3398876
Vav-Cre Mta2 $^{f/f}$ _(918t4)_pre-B	This Paper	GSM3398877
Vav-Cre Mta2 $^{f/f}$ _(918t6)_pre-B	This Paper	GSM3398878
Vav-Cre Mta2 $^{f/f}$ _(931t14)_pre-B	This Paper	GSM3398879
INPUT_697	This Paper	GSM2882822
AIOLOS_697	This Paper	GSM2882823
IKAROS_697	This Paper	GSM2882824
MTA2_697	This Paper	GSM2882825
Mi2_697	This Paper	GSM2882826
OCAB_697	This Paper	GSM2882827
OCT2_697	This Paper	GSM2882828
HDAC2_697	This Paper	GSM3398902
Experimental Models: Cell Lines		
697 human pre-B acute lymphoblastic leukemia cell line	DSMZ	Cat# ACC42
Namalwa Burkitt's lymphoma cell line	ATCC	Cat# CRL-1432^{TM}
Experimental Models: Organisms/Strains		
Mta2 conventional null mice	Lu et al., 2008	N/A
Cd19-Cre transgenic mice	The Jackson Lab	Stock # 004126
Mb1-Cre transgenic mice	The Jackson Lab	Stock # 020505
Mx-Cre transgenic mice	The Jackson Lab	Stock # 003556
Vav1-Cre transgenic mice	The Jackson Lab	Stock # 008610
Oca-B null mice	Kim et al., 1996	N/A
Oligonucleotides		
sh_hOCA-B#1	Sigma-Aldrich	Cat# TRCN0000431764
5′-AAATGAAAGCCCATGGACCAC-3′		
Sh_hOCA-B#2	Sigma-Aldrich	Cat# TRCN0000423580
5′-AAATCCCTATAATTACCTCCC-3′		
Scramble shRNA	Sigma-Aldrich	Cat# SHC002
5′-CAACAAGATGAAGAGCACCAA-3′		
Oligonucleotides for qPCRs	This paper	Table S6
Recombinant DNA		
pLKO.1 scramble shRNA	This paper	N/A
pLKO.1 sh_hOCA-B#1	This paper	N/A
pLKO.1 sh_hOCA-B#2	This paper	N/A
Software and Algorithms		
Bowtie2	Langmead and Salzberg, 2012	http://bowtie-bio.sourceforge.net/bowtie2/index.shtml
TopHat	Kim et al., 2013	https://github.com/DaehwanKimLab/tophat2
Cufflinks	Trapnell et al., 2010	https://github.com/cole-trapnell-lab/cufflinks
edgeR	Robinson et al., 2010	http://bioconductor.org
Enrichr	Kuleshov et al., 2016	http://amp.pharm.mssm.edu/Enrichr

(*Continued on next page*)

Continued

REAGENT or RESOURCE	SOURCE	IDENTIFIER
Samtools	Li et al., 2009	http://samtools.sourceforge.net/
Homer	Heinz et al., 2010	http://homer.ucsd.edu/homer/
ngsplot	Shen et al., 2014	https://github.com/shenlab-sinai/ngsplot
Integrative Genomics Viewer (IGV)	Robinson et al., 2011	https://software.broadinstitute.org/software/igv/
GSEA	Subramanian et al., 2005	http://software.broadinstitute.org/gsea/index.jsp
Other		
Sheep Red Blood Cells	Cocalico Biologicals, Inc.	N/A
Lipopolysaccharides (LPS)	Sigma-Aldrich	Cat# L2637
Poly (I:C)	Sigma-Aldrich	Cat# P9582

LEAD CONTACT AND MATERIALS AVAILABILITY

Further information and requests for resources and reagents should be directed to and will be fulfilled by the Lead Contact, Robert G. Roeder (roeder@rockefeller.edu).

EXPERIMENTAL MODEL AND SUBJECT DETAILS

Mice

Mice were maintained in environmental control facilities at the Rockefeller University and the University of North Carolina at Chapel Hill. Mice of both sexes were 8 to 12 weeks old unless otherwise indicated. The mouse maintenance and experiments were performed following the Institutional Animal Care and Use Committee (IACUC) approved protocols of the Rockefeller University and University of North Carolina at Chapel Hill. Mice carrying *Mta2* conditional alleles ($Mta2^{fl/fl}$) were generated as described before (Lu et al., 2008). The *Cd19-Cre* mice, *Mb1-Cre* mice, *Mx1-Cre* transgenic mice, *Vav1-Cre* mice and *Oca-B* knockout (KO) mice were described previously (Hobeika et al., 2006; Kim et al., 1996; Kühn et al., 1995; Ogilvy et al., 1999; Rickert et al., 1997). The *Mta2* KO mice (Δ/Δ) were derived by crossing *EIIa-Cre* transgenic mice with $Mta2^{fl/fl}$ mice (Lu et al., 2008). *Mta2* Δ/Δ and littermate or age-matched control mice were of mixed B6/129 genetic background. The conditional KO mice had been backcrossed with C57/BL6 mice for at least six generations. For induction of *Mx1-Cre* transgene expression, *Mx1-Cre* $Mta2^{flfl}$ and littermate $Mta2^{flfl}$ mice received two intraperitoneal injections of poly (I:C) (250 μg) at day 28 and day 30 of age. Mouse genomic DNA was isolated using DNeasy Blood and Tissue Kit (QIAGEN) for genotyping. The primers for genotyping *Mta2* alleles and *Oca-B* alleles can be found in Table S6. The primers for genotyping other transgenic mouse strains described above can be found at the corresponding websites of The Jackson Laboratory (https://www.jax.org/).

Cell Line

697 cells are human pre-B leukemia cells that carry the E2A-PBX1 fusion gene (Kamps et al., 1991) and were cultured with RPMI 1640, 10% fetal bovine serum (FBS). Namalwa cells are human Burkitt's lymphoma cells and were cultured with RPMI 1640, 10% FBS.

METHOD DETAILS

Flow Cytometry

Mta2 mutant and *Oca-B* mutant mice, and littermate control or age-, sex-matched control mice were used for analysis. Single cell suspensions of bone marrow cells and spleen cells were stained with FITC-, PE-, PerCP/Cy5.5-, PE/Cy7-, Brilliant Violet 605-, and APC-conjugated monoclonal antibodies (described in Key Resources Table) and DAPI. Stained cells were analyzed with either BD LSR II or BD FACSCalibur (BD Biosciences). The cell staining and gating schemes were indicated in the figures, figure legends and results. The specific B cell populations were sorted with BD FACSAria (BD Biosciences). The flow cytometry data were analyzed using BD FACSDiva and FlowJo softwares. For FACS analyses of bone marrow B cell subpopulations, two femurs from each mouse were used for immunofluorescence staining and cell sorting.

Immunoprecipitation (IP)

Dynabeads™ Protein G beads (Invitrogen) were first washed twice with PBS containing 0.5% BSA and 0.05% Triton X-100 then incubated with specific antibodies (about 2 μg antibody for each IP assay) in the same buffer for 2 to 3 h or overnight at 4°C. The conjugated antibodies then were incubated with nuclear extracts (NE) derived from 697 cells or Namalwa cells overnight at 4°C. About 200 μg of NE was used for each IP assay. After washing with buffer BC200 [20 mM Tris (pH 7.9), 0.2 mM EDTA, 1 mM DTT, 0.2 mM PMSF, 20% glycerol, and 200 mM of KCl] for three times, the immunoprecipitates were subject to immunoblot.

RNA isolation and reverse transcription (RT)

Total RNA was isolated from sorted primary B cells or cultured 697 cells using Arcturus™ PicoPure RNA isolation Kit (Applied Biosystems). For each sample, 40 to 100 μg RNA was used for reverse transcription using qScript cDNA SuperMix (Quanta Biosciences) according to Manufacturer's instruction.

Quantitative PCR

Quantitative PCR (qPCR) assays were performed in triplicate using QuaniTect SYBR Green PCR mix (QIAGEN) on a 7300 Real Time PCR System (Applied Biosystems). The numbers of biological samples and independent experiments used for qPCR analyses are indicated in the figure legends and text. mRNA levels were normalized to the expression level of *Hprt* (*HPRT*) or *Gapdh* (*GAPDH*) gene in mouse and human cells. For deletion efficiency and immunoglobulin gene rearrangement analyses, genomic DNA amounts were normalized to promoter regions of *Cd79b* or *Cdk6* genes. Primer sequences for RT-qPCR and qPCR are listed in Table S6.

RNA-seq and gene ontology

For pro-B cell gene profiling, $B220^+IgM^-CD43^+$ pro-B cells from 2 pairs of 10-week-old *Vav-Cre Mta2*$^{fl/fl}$ and littermate control mice were sorted for RNA isolation. For pre-B cell gene profiling, $B220^+IgM^-CD43^-$ small pre-B cells from 3 pairs of 10-week-old *Vav-Cre Mta2*$^{fl/fl}$ and littermate control mice were sorted for RNA isolation. The RNA library preparation was done with TruSeq Stranded mRNA Prepration Kit (Illumina). The sequencing was done by the Genomics Core Facility at The Rockefeller University using an Illumina HiSeq 2500 Sequencer. Sequencing data were aligned to mm10 reference genome on Galaxy (https://usegalaxy.org/) with default parameters using TopHat software (Kim et al., 2013). The aligned sequences were assembled using Cufflinks and then analyzed using edgeR package in R script (Robinson et al., 2010; Trapnell et al., 2010). The cut-off line for differential gene expression levels was 1.5 fold with p values smaller than 0.05. Enrichr (http://amp.pharm.mssm.edu/Enrichr/) was used for gene ontology analysis and GSEA was used for gene set enrichment analysis (Kuleshov et al., 2016; Subramanian et al., 2005).

Genomic rearrangement of the Immunoglobulin heavy chain and light chain loci

$B220^+IgM^-CD43^+$ pro-B and $B220^+IgM^-CD43^-$ small pre-B cells from 4 pairs of 8 to 12-week-old *Vav-Cre Mta2*$^{fl/fl}$ and littermate control mice were sorted, and the genomic DNA was isolated using DNeasy Blood and Tissue Kit (QIAGEN). The $V_H(D)J_H$ recombination efficiencies in pro-B cells were measured by qPCR using primers indicated in Figure 2E and described in Table S6. The V_KJ_K recombination efficiencies in pre-B cells were measured by qPCR using primers indicated in Figure 2G and described in Table S6. A universal V_k primer was used in combination with a J_k1, J_k2, J_k4 or J_k5 primer. Promoter regions of *Cd79b* or *Cdk6* genes were used to normalize genomic DNA amounts of different samples. The number of samples used in the assays can be found in the corresponding Figure Legends.

Chromatin immunoprecipitation (ChIP) and ChIP-sequencing

The antibodies used for ChIP are described in Key Resources Table. Normal rabbit IgG (sc-2027, Santa Cruz Biotechnology Inc.) was used as an immunoprecipitation control. In ChIP experiments, cells were incubated sequentially, at room temperature (RT), for 30 min in 2mM disuccinimidyl glutarate (DSG), for 10 min after formaldehyde addition to a final concentration of 1%, and for 5 min after addition of glycine to a final concentration of 125mM. Fixed cells were washed twice with cold PBS and resuspended in RIPA 0.3 buffer (0.1% SDS, 1% Triton X-100, 10mM Tris-HCl(pH7.4), 1mM EDTA (pH8.0), 0.1% Sodium Deoxycholate, and 0.3M NaCl). The antibodies and IgG were first incubated with Dynabeads Protein G (Invitrogen) at 4°C overnight, then washed and then incubated with sonicated cell lysate (1-2ug antibody for a ChIP-qPCR, 6-10ug antibody for ChIP-seq) at 4° overnight. For reverse crosslinking, the beads were first washed 4-8 times with high salt buffer (20mM Tris pH8, 2mM EDTA, 0.1%SDS, 1%TX100, 500mM NaCl), then washed with TE buffer (pH8.0) and then washed with elution buffer (1% SDS in TE buffer) for 15 min at RT. Eluates were then incubated at 65°C for 4 h after addition of NaCl and RNase to final concentrations of 200mM and 4ug/ml and then at 55°C for 1 h after addition of proteinase K to100ug/ml. Finally, the immunoprecipitated DNA samples were purified by QIAquick PCR Purification Kit (QIAGEN) for further analysis. About 2–5 ng of DNA precipitated by ChIP was used as the starting material for the generation of single-end sequencing libraries as described (Yu et al., 2015). Cluster generation and sequencing was performed by the Genomics Resource Center at The Rockefeller University with a HiSeq 2500 system with a read length of 50 nucleotides according to the manufacturer's guidelines (Illumina).

Data analysis for ChIP-seq

The softwares used for ChIP-seq data analyses are listed in Key Resources Table. In brief, sequencing data were aligned using Bowtie2 (Langmead and Salzberg, 2012) to hg19 version of the reference genome on Galaxy (https://usegalaxy.org/) with default parameters. Duplicate mapped reads were removed using Samtools with the rmdup option. Bedgraph files were generated by Homer using makeUCSCfile program with default parameters (Li et al., 2009). ChIP-seq tracks generated by converting bedgraph files to tdf formats were displayed by IGV software (Robinson et al., 2011). Peak files were generated by Homer using findPeaks program with default parameters (Heinz et al., 2010). The threshold for statistical significance of peaks was set at 10^{-10}. Annotation of filtered peaks was done by Homer with annotatePeaks program with default parameters except -style factor. ChIP-seq signals at TSSs were plotted as averaged profiles or heatmaps by ngsplot with parameter -SC global -GO max. ChIP-seq signals at enhancers

were plotted as averaged profiles by ngsplot with parameter -L 10000 -F Gm12878 -SC global -GO max (Shen et al., 2014). Motif analyses were performed by Homer using findMotifsGenome program with default parameters.

shRNA knockdown

For knockdown of the *OCA-B* gene, $1x10^7$ 697 cells were infected with lentivirus carrying OCA-B shRNA sequences or scramble RNA sequence plus 8 μg/ml polybrene in RPMI 1640 medium with 10% FBS. After 12 h, the infected cells were changed to fresh medium with 10% FBS and cultured for 2 days. The cells were then treated with 1 μg/ml puromycin and cultured for another 2 days. Total RNAs were isolated for measuring expression levels of OCA-B by RT-qPCR.

Immunization and immunoglobulin (Ig) class switch

Sheep red blood cells (SRBC) were washed with PBS and 1:10 diluted in PBS. 500 μL diluted SRBC were intraperitoneal injected to each mouse. Splenic cells were isolated on day 9 or day 10 after immunization for FACS analysis of germinal center B cells. For *Ig* class switch assay, naive splenic B cells were enriched by negative selection using anti-CD43 conjugated magnetic beads (Miltenyi Biotec). Isolated cells, at a concentration of 300 to 500K cell per ml, were incubated in RPMI 1640 medium with 10% FCS. *Ig* class switching were induced by 5ng/ml IL-4 (Sigma) + 25ug/ml LPS (Sigma) (for *IgG1*), 25ug/ml LPS (for *IgG3*), and 5ng/ml IL-4 + 0.2mg/ml anti-CD40 antibody (BioLegend) + 0.1ng/ml TGF-β (BioLegend) (for *IgA*) respectively. After incubation for three days, the cells were analyzed by flow cytometry for specific Ig surface markers.

QUANTIFICATION AND STATISTICAL ANALYSIS

All data were analyzed using Excel or GraphPad Prism softwares. t tests were used for calculation of statistical significance when comparing data from two groups. Differences were considered significant when p values were < 0.05. p values are depicted in figures using one to three asterisks ($*p < 0.05$, $**p < 0.01$, and $***p < 0.005$). Data are presented as mean + SD with n indicating the number of animals or independent experiments if not stated otherwise in the figure legends or in the text.

DATA AND CODE AVAILABILITY

The RNA-seq and ChIP-seq data have been deposited in NCBI Gene Expression Omnibus. The accession number for the RNA-seq data reported in this paper is GSE107885, and the accession number for the ChIP-seq data reported in this paper is GSE107886.

Cell Reports, Volume *28*

Supplemental Information

MTA2/NuRD Regulates B Cell Development and Cooperates with OCA-B in Controlling the Pre-B to Immature B Cell Transition

Xiangdong Lu, Chi-Shuen Chu, Terry Fang, Violeta Rayon-Estrada, Fang Fang, Alina Patke, Ye Qian, Stephen H. Clarke, Ari M. Melnick, Yi Zhang, F. Nina Papavasiliou, and Robert G. Roeder

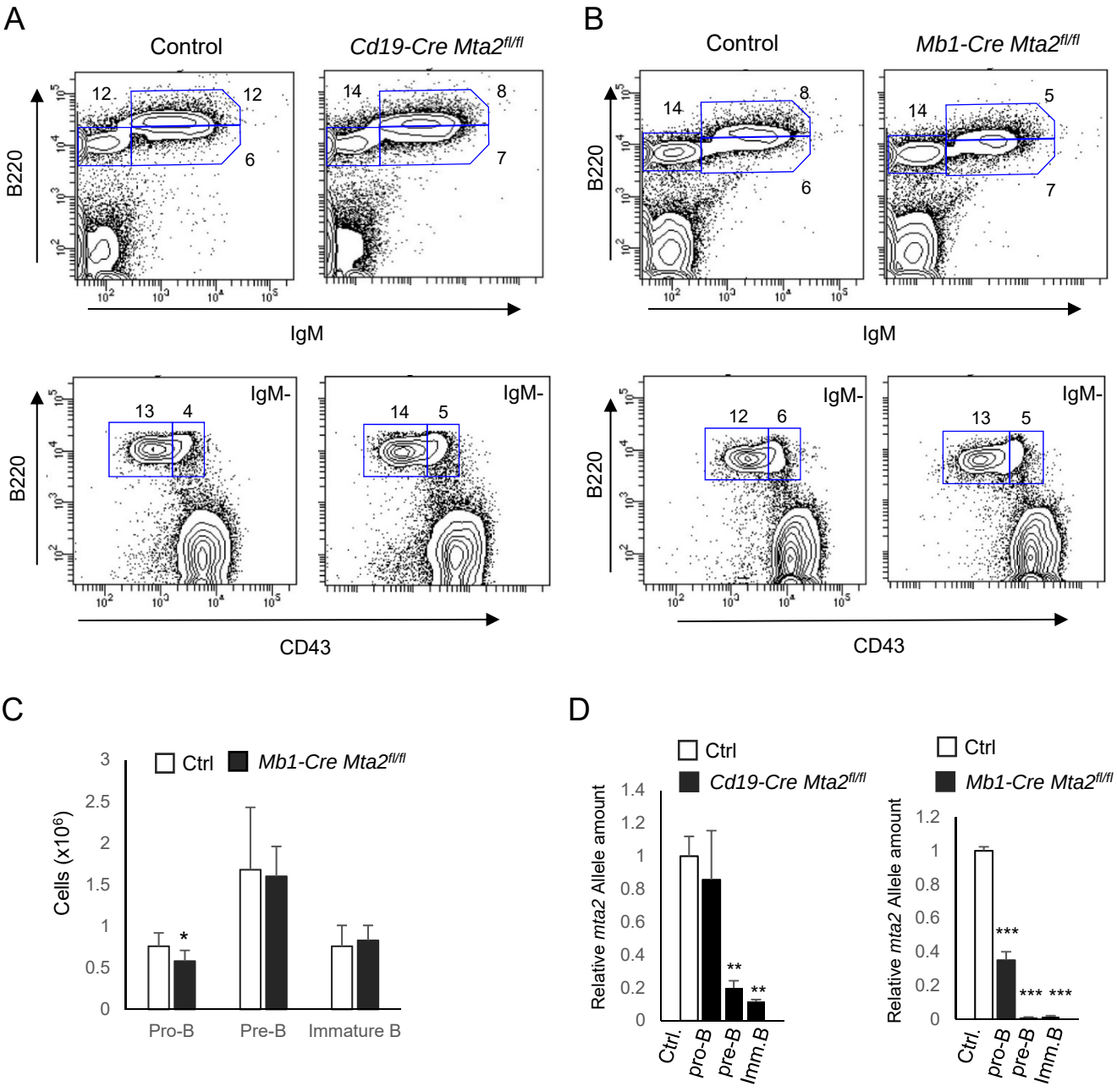

Figure S1. B cell-specific *Mta2* KO mice do not recapitulate BM phenotypes of conventional *Mta2* KO mice. Related to Figure 1 and 2.

(A, B) FACS analysis of BM B cells from *Cd19-Cre Mta2*$^{fl/fl}$ vs control (A) and *Mb1-Cre Mta2*$^{fl/fl}$ vs control mice (B). (C) Numbers of BM B cell subpopulations in *Mb1-Cre Mta2*$^{fl/fl}$ and control (Ctrl) mice (two femurs). (n=7 for each genotype, t-test, *p<0.05). (D) Quantitative PCR (qPCR) results show efficiencies of Cd19-Cre-mediated (left panel) and Mb1-Cre-mediated (right panel) deletion of the *Mta2* allele in indicated cell populations (data from 3 control mice, 4 *Cd19-Cre Mta2*$^{fl/fl}$ mice, and 3 *Mb1-Cre Mta2*$^{fl/fl}$ mice, t-test, **p< 0.01, ***p< 0.001).

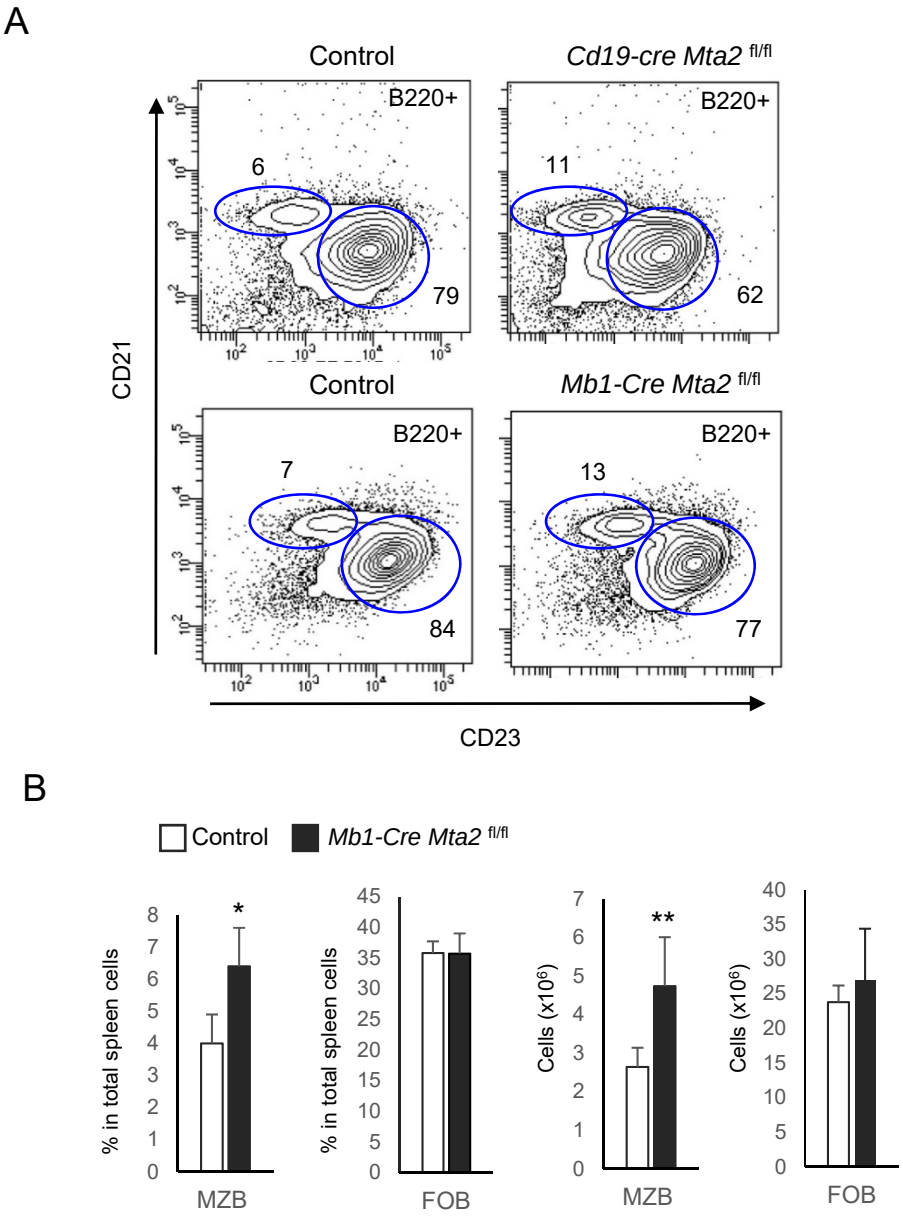

Figure S2. B cell-specific inactivation of the *Mta2* gene leads to an increase in the MZB population. Related to Figure 1 and 2. (A) Representative FACS analyses of MZB and FOB cells from *Cd19-Cre Mta2*$^{fl/fl}$, *Mb1-Cre Mta2*$^{fl/fl}$ and control mice. (B) Percentages (left panels) and numbers (right panels) of MZB and FOB cells from *Mb1-Cre Mta2*$^{fl/fl}$ and control mice (n=6 for each genotype; t-test, *p<0.05, **p<0.01).

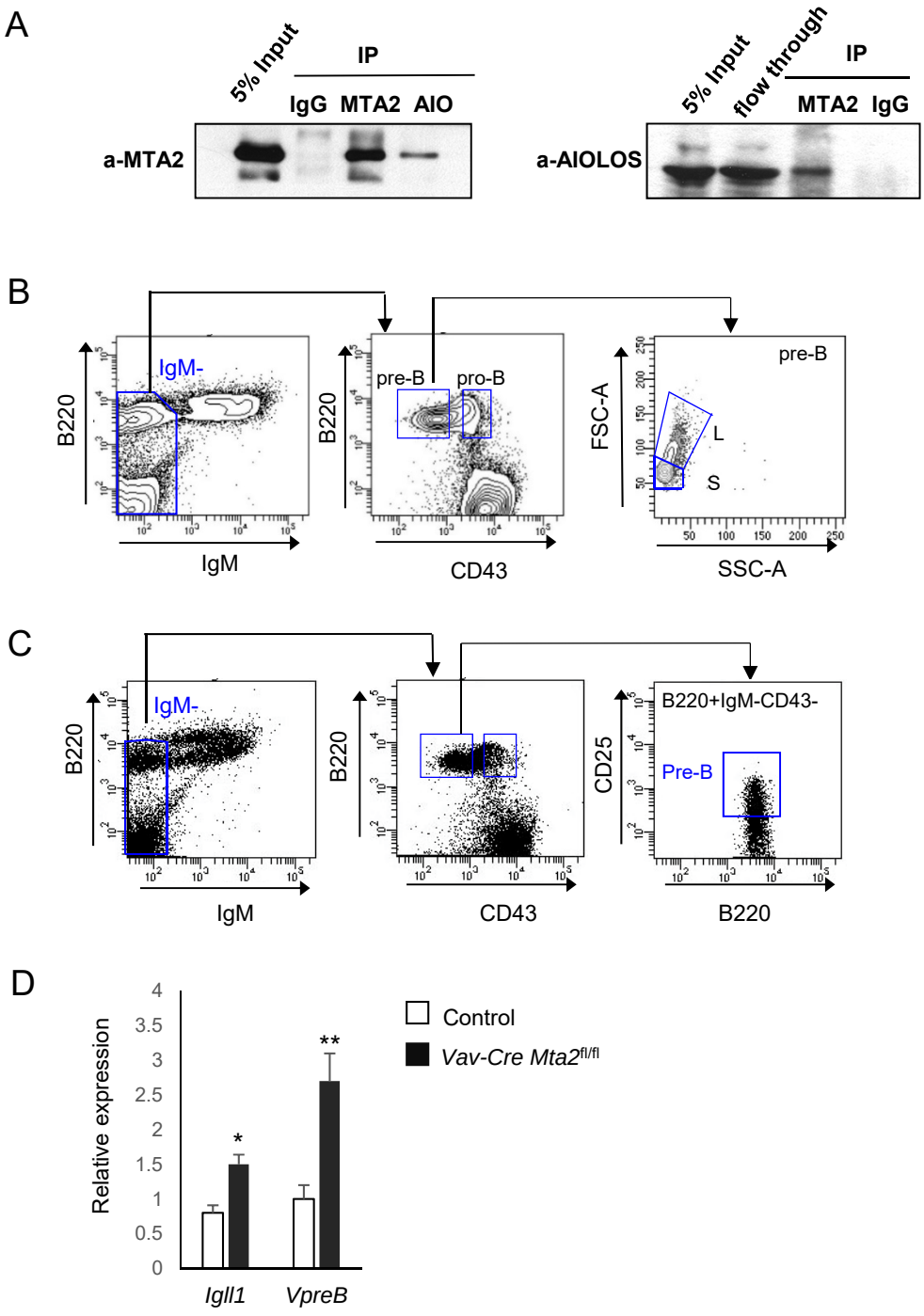

Figure S3. MTA2 interacts with AIOLOS and represses pre-BCR genes. Related to Figure2 and 3.

(A) Co-immunoprecipitation of Mta2 and Aiolos from Namalwa cell nuclear extract using anti-MTA2, anti-Aiolos and rabbit IgG antibodies. Proteins detected by immunoblot. (B) FACS gating schemes for sorting pro-B cells ($B220^{+}IgM^{-}CD43^{+}$), pre-B cells ($B220^{+}IgM^{-}CD43^{-}$) and small pre-B cells (L stands for large pre-B cells, S stands for small pre-B cells). (C) An alternative FACS gating scheme for sorting pre-B cell ($B220^{+}IgM^{-}CD43^{-}CD25^{+}$). (D) RT-qPCR analysis using the pre-B cell sorting scheme shown in panel C. (n=4 for each genotype, t-test *p<0.05, **p<0.01).

A

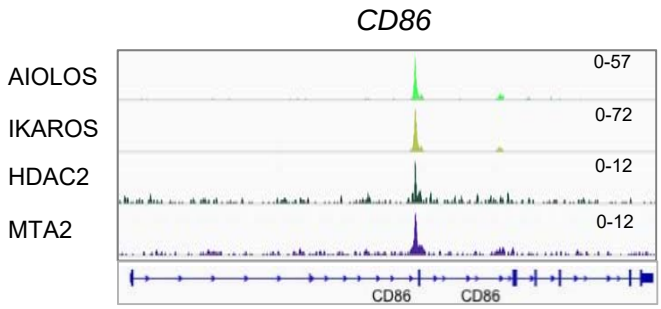

B

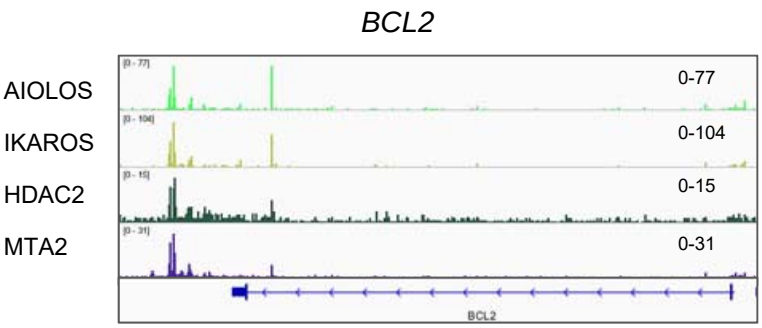

Figure S4. MTA2/HDAC2 and AIOLOS/IKAROS binding at non-promoter regions. Related to Figure 4.

(A, B) Snapshots of AIOLOS, IKAROS, HDAC2 and MTA2 binding at *CD86* gene intronic elements (A) and at *BCL2* gene intronic and 3' regulatory (but not promoter) elements (B) in 697 cells.

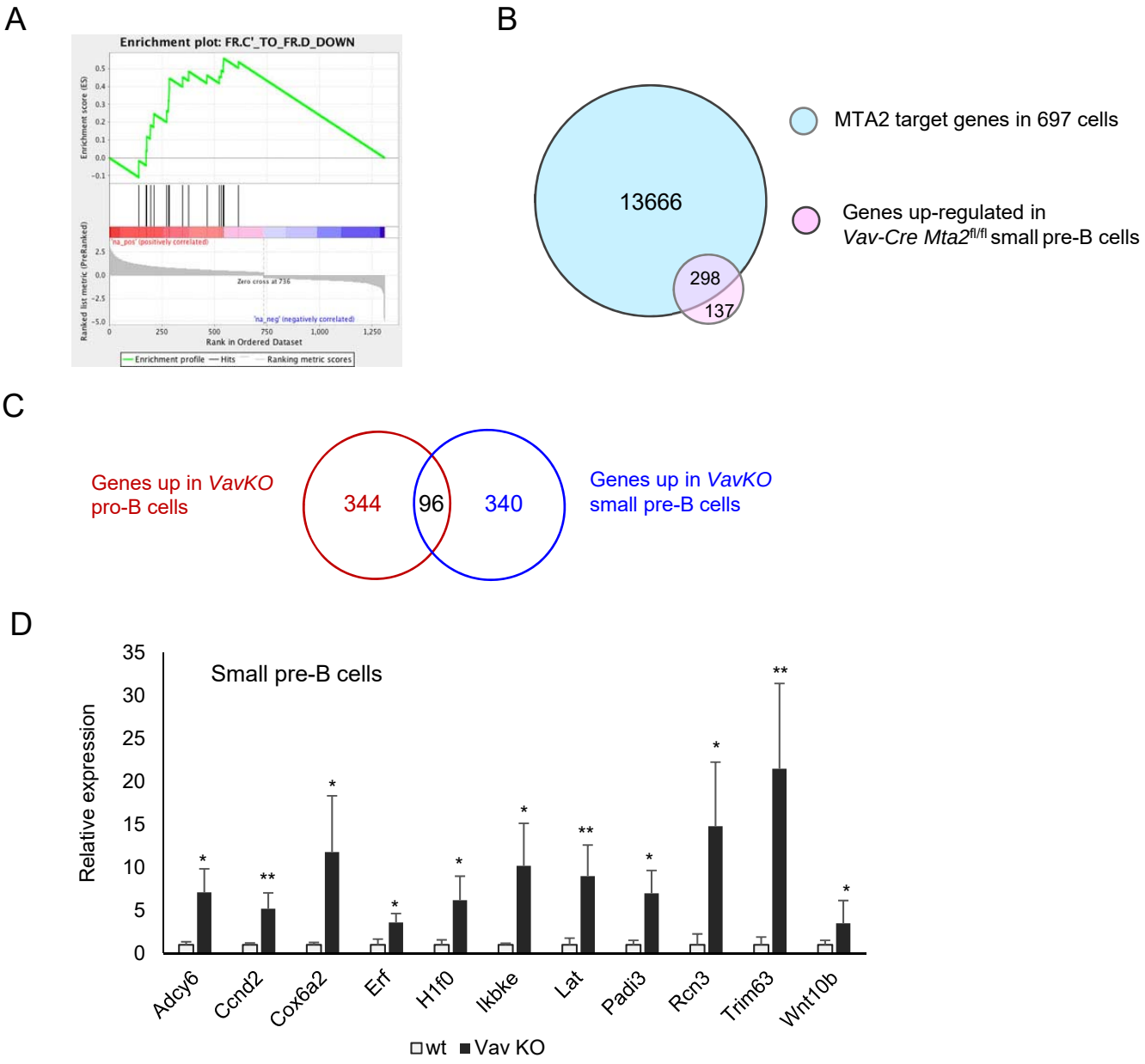

Figure S5. MTA2-regulated genes in mouse pro-B and pre-B cells. Related to Figure 4 and 5.

(A) GSEA analysis of genes up-regulated in Mta2-deficient pre-B cells relative to genes that show decreased expression during BM B cell development from Hardy Fr C' to Fr D stages. (B) Overlap between MTA2-bound genes identified in 697 cells and human orthologs of mouse genes up-regulated in *Vav-Cre Mta2*$^{fl/fl}$ pre-B cells relative to control pre-B cells. Among the latter group, about 65% (378 out of 578) are potential direct Mta2 target genes. (C) Overlap between up-regulated genes in MTA2-deficient pro-B cells and those in MTA2-deficient small pre-B cells. (D) Validation by RT-qPCR of selected genes identified by RNA-seq as up-regulated genes in MTA2-deficent small pre-B cells. The means and standard deviations are derived from 3 pairs of *Vav-Cre Mta2*$^{fl/fl}$ (VavKO) and control mice (different from the cohorts used for RNA-seq analyses) (t-test *p<0.05, **p<0.01).

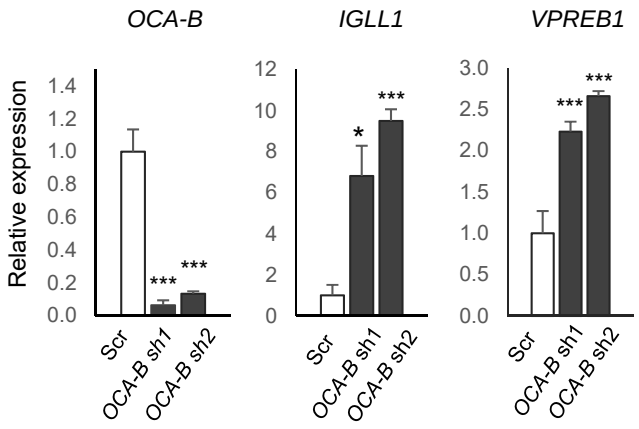

Figure S6. *OCA-B* Knockdown-mediated up-regulation of pre-BCR genes in human pre-B cells. Related to Figure 6. RT-qPCR results of relative expression level of *IGLL1, VPREB1* and *OCA-B* in 697 cells treated with *OCA-B* shRNAs and scramble shRNA. The means were obtained from triplicated PCR reactions (t-test, n=3, *p<0.05, ***p<0.001).

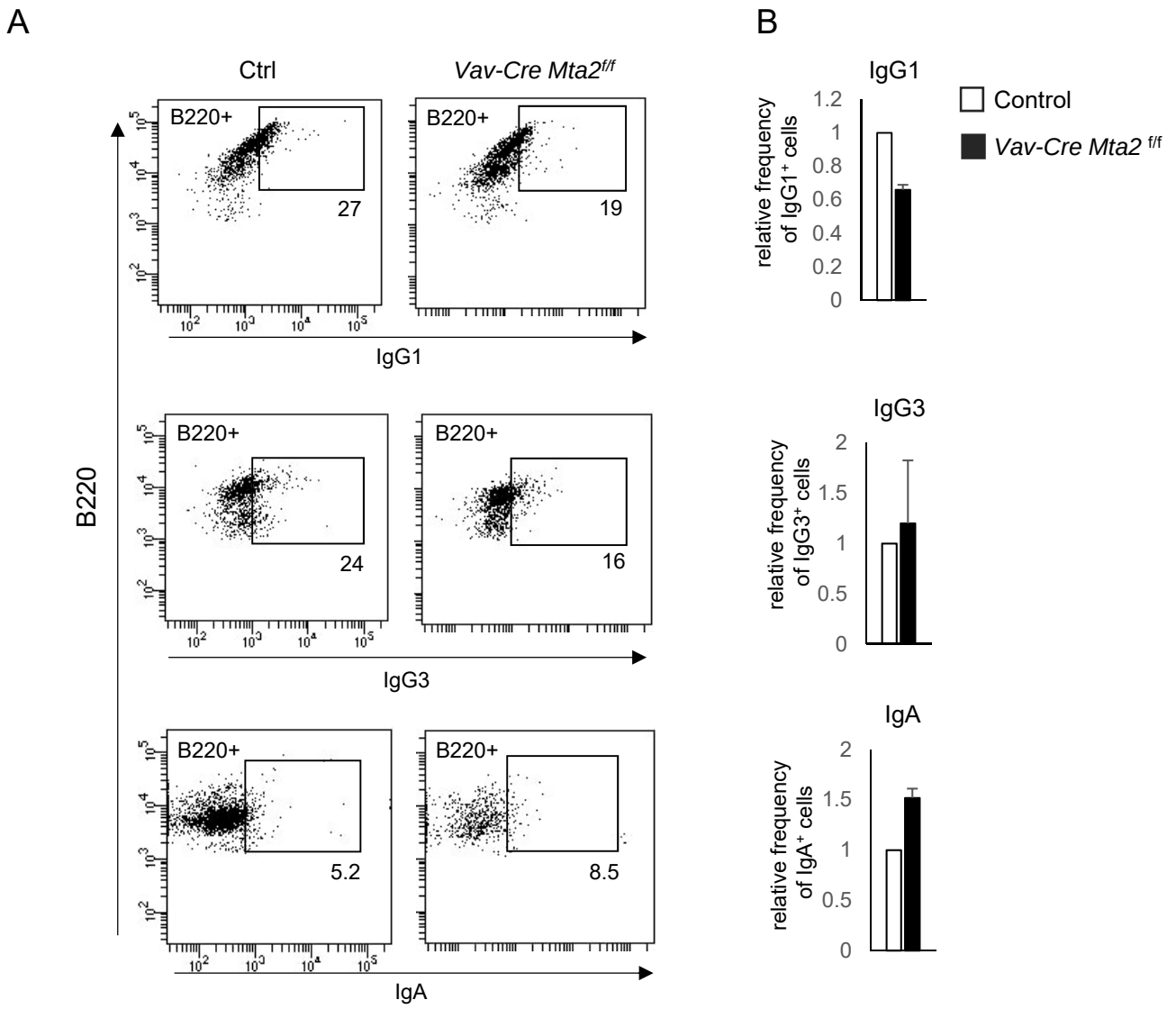

Figure S7. Loss of MTA2 activity causes abnormal immunoglobulin class switching. Related to Figure 7.
(A) FACS data show surface expression of IgG1, IgG3, and IgA on stimulated splenic B cells. Cells were stimulated by IL-4+LPS (to induce IgG1), LPS only (to induce IgG3), and IL-4+anti-CD40+TGFb (to induce IgA), respectively. Numbers indicate the percentages of surface Ig-expressing cells among B220 positive cells. (B) Relative average percentages of Ig-expressing cells in splenic B cells from 3 pairs of *Vav-Cre Mta2*$^{f/f}$ and litter mate control mice are presented. The data are normalized to percentages of Ig-expressing cells in splenic B cells in control samples.

Table S1. DNA motifs recognized by AIOLOS in human pre-B cells. Related to Figure 4.

Rank	Motif	P-value	log P-pvalue	% of Targets	% of Background	STD(Bg STD)	Best Match/Details	Motif File
1		1e-1484	-3.418e+03	36.07%	16.84%	50.6bp (59.6bp)	Etv2(ETS)/ES-ER71-ChIP-Seq(GSE59402)/Homer(0.967) (0.980) More Information | Similar Motifs Found	motif file (matrix)
2		1e-1379	-3.176e+03	24.08%	9.02%	51.6bp (58.4bp)	RUNX1(Runt)/Jurkat-RUNX1-ChIP-Seq(GSE29180) /Homer(0.944) More Information | Similar Motifs Found	motif file (matrix)
3		1e-1296	-2.985e+03	24.69%	9.75%	49.0bp (58.3bp)	EBF(EBF)/proBcell-EBF-ChIP-Seq(GSE21978)/Homer(0.973) More Information | Similar Motifs Found	motif file (matrix)
4		1e-611	-1.408e+03	7.14%	1.89%	54.9bp (58.2bp)	BORIS(Zf)/K562-CTCFL-ChIP-Seq(GSE32465)/Homer(0.915) More Information | Similar Motifs Found	motif file (matrix)
5	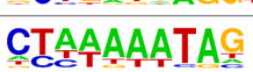	1e-425	-9.798e+02	11.18%	4.99%	55.0bp (58.9bp)	Mef2c(MADS)/GM12878-Mef2c-ChIP-Seq(GSE32465) /Homer(0.950) More Information | Similar Motifs Found	motif file (matrix)
6		1e-278	-6.421e+02	3.12%	0.79%	54.4bp (52.3bp)	Atf3(bZIP)/GBM-ATF3-ChIP-Seq(GSE33912)/Homer(0.995) More Information | Similar Motifs Found	motif file (matrix)
7		1e-276	-6.374e+02	21.58%	14.20%	54.5bp (57.2bp)	E2A(bHLH)/proBcell-E2A-ChIP-Seq(GSE21978)/Homer(0.967) More Information | Similar Motifs Found	motif file (matrix)
8		1e-136	-3.144e+02	5.91%	3.18%	55.2bp (65.6bp)	IRF2(IRF)/Erythroblas-IRF2-ChIP-Seq(GSE36985) /Homer(0.866) More Information | Similar Motifs Found	motif file (matrix)
9		1e-125	-2.880e+02	23.23%	17.95%	55.2bp (60.7bp)	Znf263(Zf)/K562-Znf263-ChIP-Seq(GSE31477)/Homer(0.737) More Information | Similar Motifs Found	motif file (matrix)
10		1e-106	-2.447e+02	1.58%	0.50%	54.7bp (59.3bp)	GFY(?)/Promoter/Homer(0.979) More Information | Similar Motifs Found	motif file (matrix)

Table S2. DNA motifs recognized by IKAROS in human pre-B cells. Related to Figure 4.

Rank	Motif	P-value	log P-pvalue	% of Targets	% of Background	STD(Bg STD)	Best Match/Details	Motif File
1		1e-2023	-4.660e+03	20.75%	6.62%	46.7bp (57.3bp)	EBF(EBF)/proBcell-EBF-ChIP-Seq(GSE21978)/Homer(0.981) More Information | Similar Motifs Found	motif file (matrix)
2		1e-1686	-3.883e+03	27.46%	11.87%	52.4bp (58.7bp)	RUNX1(Runt)/Jurkat-RUNX1-ChIP-Seq(GSE29180) /Homer(0.982) More Information | Similar Motifs Found	motif file (matrix)
3		1e-1587	-3.655e+03	35.83%	18.46%	51.3bp (60.1bp)	ERG(ETS)/VCaP-ERG-ChIP-Seq(GSE14097)/Homer(0.977) More Information | Similar Motifs Found	motif file (matrix)
4		1e-1500	-3.455e+03	7.45%	1.13%	52.8bp (56.0bp)	CTCF(Zf)/CD4+-CTCF-ChIP-Seq(Barski_et_al.)/Homer(0.918) More Information | Similar Motifs Found	motif file (matrix)
5		1e-470	-1.084e+03	8.09%	3.37%	55.7bp (56.6bp)	MEF2D/MA0773.1/Jaspar(0.963) More Information | Similar Motifs Found	motif file (matrix)
6		1e-382	-8.797e+02	3.94%	1.19%	54.1bp (53.7bp)	Atf3(bZIP)/GBM-ATF3-ChIP-Seq(GSE33912)/Homer(0.994) More Information | Similar Motifs Found	motif file (matrix)
7		1e-294	-6.791e+02	13.33%	8.12%	54.3bp (58.3bp)	Tcf12(bHLH)/GM12878-Tcf12-ChIP-Seq(GSE32465) /Homer(0.975) More Information | Similar Motifs Found	motif file (matrix)
8		1e-245	-5.659e+02	17.94%	12.35%	53.1bp (61.5bp)	E2F1(E2F)/Hela-E2F1-ChIP-Seq(GSE22478)/Homer(0.748) More Information | Similar Motifs Found	motif file (matrix)
9		1e-157	-3.616e+02	11.22%	7.60%	54.5bp (60.2bp)	PB0076.1_Sp4_1/Jaspar(0.782) More Information | Similar Motifs Found	motif file (matrix)
10		1e-155	-3.585e+02	14.01%	9.97%	55.1bp (63.6bp)	IRF1(IRF)/PBMC-IRF1-ChIP-Seq(GSE43036)/Homer(0.842) More Information | Similar Motifs Found	motif file (matrix)

Table S3. DNA motifs recognized by MTA2 in human pre-B cells. Related to Figure 4.

Rank	Motif	P-value	log P-pvalue	% of Targets	% of Background	STD(Bg STD)	Best Match/Details	Motif File
1		1e-1254	-2.888e+03	18.90%	5.10%	46.2bp (55.3bp)	EBF(EBF)/proBcell-EBF-ChIP-Seq(GSE21978)/Homer(0.991) More Information | Similar Motifs Found	motif file (matrix)
2		1e-822	-1.894e+03	21.17%	8.31%	52.5bp (59.7bp)	RUNX1(Runt)/Jurkat-RUNX1-ChIP-Seq(GSE29180) /Homer(0.944) More Information | Similar Motifs Found	motif file (matrix)
3		1e-733	-1.690e+03	30.35%	15.41%	53.5bp (58.1bp)	Fli1(ETS)/CD8-FLI-ChIP-Seq(GSE20898)/Homer(0.987) More Information | Similar Motifs Found	motif file (matrix)
4		1e-426	-9.817e+02	5.13%	1.07%	54.1bp (58.3bp)	BORIS(Zf)/K562-CTCFL-ChIP-Seq(GSE32465)/Homer(0.926) More Information | Similar Motifs Found	motif file (matrix)
5		1e-200	-4.627e+02	5.61%	2.20%	56.7bp (58.2bp)	Mef2c(MADS)/GM12878-Mef2c-ChIP-Seq(GSE32465) /Homer(0.969) More Information | Similar Motifs Found	motif file (matrix)
6		1e-188	-4.342e+02	8.19%	3.98%	53.5bp (56.4bp)	AP-1(bZIP)/ThioMac-PU.1-ChIP-Seq(GSE21512)/Homer(0.970) More Information | Similar Motifs Found	motif file (matrix)
7		1e-157	-3.626e+02	14.29%	8.97%	53.6bp (58.7bp)	E2A(bHLH)/proBcell-E2A-ChIP-Seq(GSE21978)/Homer(0.973) More Information | Similar Motifs Found	motif file (matrix)
8		1e-91	-2.105e+02	8.90%	5.63%	53.9bp (58.9bp)	E2F6/MA0471.1/Jaspar(0.766) More Information | Similar Motifs Found	motif file (matrix)
9		1e-76	-1.755e+02	1.25%	0.34%	54.8bp (60.3bp)	GFY(?)/Promoter/Homer(0.989) More Information | Similar Motifs Found	motif file (matrix)
10		1e-74	-1.713e+02	9.63%	6.52%	55.1bp (64.6bp)	PB0159.1_Rfx4_2/Jaspar(0.696) More Information | Similar Motifs Found	motif file (matrix)

Table S4. DNA motifs recognized by HDAC2 in human pre-B cells. Related to Figure 4.

Rank	Motif	P-value	log P-pvalue	% of Targets	% of Background	STD(Bg STD)	Best Match/Details	Motif File
1		1e-398	-9.184e+02	19.82%	5.30%	48.3bp (56.2bp)	EBF(EBF)/proBcell-EBF-ChIP-Seq(GSE21978)/Homer(0.946) More Information | Similar Motifs Found	motif file (matrix)
2		1e-253	-5.842e+02	27.81%	12.67%	53.6bp (57.5bp)	RUNX1(Runt)/Jurkat-RUNX1-ChIP-Seq(GSE29180) /Homer(0.963) More Information | Similar Motifs Found	motif file (matrix)
3		1e-226	-5.219e+02	29.85%	14.86%	54.2bp (57.2bp)	Etv2(ETS)/ES-ER71-ChIP-Seq(GSE59402)/Homer(0.967)(0.983) More Information | Similar Motifs Found	motif file (matrix)
4		1e-88	-2.045e+02	11.30%	5.25%	54.1bp (59.8bp)	Mef2c(MADS)/GM12878-Mef2c-ChIP-Seq(GSE32465) /Homer(0.961) More Information | Similar Motifs Found	motif file (matrix)
5		1e-76	-1.759e+02	24.15%	15.66%	54.1bp (57.9bp)	Ptf1a(bHLH)/Panc1-Ptf1a-ChIP-Seq(GSE47459)/Homer(0.944) More Information | Similar Motifs Found	motif file (matrix)
6		1e-58	-1.352e+02	17.73%	11.23%	55.3bp (62.3bp)	MF0009.1_TRP(MYB)_class/Jaspar(0.843) More Information | Similar Motifs Found	motif file (matrix)
7		1e-50	-1.158e+02	4.56%	1.77%	56.0bp (54.5bp)	Atf3(bZIP)/GBM-ATF3-ChIP-Seq(GSE33912)/Homer(0.981) More Information | Similar Motifs Found	motif file (matrix)
8		1e-23	-5.459e+01	17.28%	13.07%	56.2bp (59.9bp)	YY2/MA0748.1/Jaspar(0.653) More Information | Similar Motifs Found	motif file (matrix)
9		1e-22	-5.094e+01	5.04%	2.90%	55.9bp (56.7bp)	TCF7L2/MA0523.1/Jaspar(0.910) More Information | Similar Motifs Found	motif file (matrix)
10		1e-21	-4.946e+01	19.35%	15.12%	55.5bp (58.4bp)	Egr2(Zf)/Thymocytes-Egr2-ChIP-Seq(GSE34254)/Homer(0.792) More Information | Similar Motifs Found	motif file (matrix)

Table S5. Inactivation of *Mta2* Gene or *Aiolos* Gene Causes Similar Defects in the Immune System. Related to Figure 1, 2, 3, S3, 6, and 7.

Phenotypes	*Mta2* KO	*Aiolos* KO
T cell hyperproliferation	+	+
Lupus-like glumerulonephritis	+	+
Production of anti-dsDNA and anti-Sm autoantibodies	+	+
Loss of Marginal Zone (MZ) B cells	+	+
*Derepression of *Igll1* and *VpreB1* expression in pre-B cells	+	+
*Synergy with OCA-B in repression of *Igll1* and *VpreB1* expression in pre-B cells	+	+
*Substantial loss of immature B, recirculating B, and splenic B cells in the absence of OCA-B	+	+
Enhanced BCR-mediated in vitro proliferation	N.D.	+
*Increased germinal center response	+	+
Decreased pro-B and pre-B populations in bone marrow	+	-
B cell lymphomagenesis	-	+

* The data were obtained from *Vav-Cre Mta2*$^{fl/fl}$ mice. N.D., not determined.

Table S6 Oligonucleotides. Related to Figure 1, 2, 3, 6, S1, S3, S5, and S6.

ChIP primers for human genes	
hIgll1-ChIP-F1	5'-CAC AGC AGG GCA GTT GGC AGA TG-3'
hIgll1-ChIP-R1	5'-CGC TGG CAG CAG CTG TCC CAT TG-3'
hVpreB1-ChIP-F1	5'-TCCTCCCTGAATGCTTCCATA-3'
hVpreB1-ChIP-R1	5'-GGCCACTACCATCCCAGACTT-3'
hCNAP1-ChIP-F1	5'-ATG GTT GCC ACT GGG GAT CT-3'
hCNAP1-ChIP-R1	5'-TGC CAA AGC CTA GGG GAA GA-3'
ChIP primers for mouse genes	
mIgll1-ChIP-F1	5'-CTGTGAGTGAAAACAGTTAGGCTTGC-3'
mIgll1-ChIP-R1	5'-ACCAGCAGGCACACCCCAGTG-3'
mVpreB1-ChIP-F1	5'-CATCAGCCACCATTAGCATC-3'
mVpreB1-ChIP-R1	5'-ACCCTGGTGCTTGTCTGAGT-3'
mCd79b-ChIP-F1	5'-GCAAGCAGAAATGTGACAGC-3'
mCd79b-ChIP-R1	5'-GATGATGAGGAGGGTCTGGA-3'
mCdk6-ChIP-F1	5'-GCCCAAGTTCAGTTCTCAGC-3'
mCdk6-ChIP-F2	5'-CGTCTCTGTGTGTGGGAATG-3'
Primers for human gene expression	
hIgll1-RT-F	5'-ACCCAGCTCACCGTTTTAAGT-3'
hIgll1-RT-R	5'-GGTCACCGTCAAGATTCCCG-3'
hVpreB1-RT-F1	5'-CGACCATGACATCGGTGTGTA-3'
hVpreB1-RT-R1	5'-GGCTCTTGTCTGATTGTGAGAA-3'
hHPRT-RT-F1	5'-CCTGGCGTCGTGATTAGTGAT-3'
hHPRT-RT-R1	5'-AGACGTTCAGTCCTGTCCATAA-3'
hGAPDH-RT-F	5'-TGTGGGCATCAATGGATTTGG-3'
hGAPDH-RT-R	5'-ACACCATGTATTCCGGGTCAAT-3'
Primers for mouse gene expression	
mIgll1-RT-F	5'-GAGACAACCCAACCCTCCAA-3'
mIgll1-RT-R	5'-TGAGGCATCCACTGGTCAGA-3'
mVpreB1-RT-F1	5'-GCTGCTGGCCTATCTCACAG-3'
mVpreB1-RT-R1	5'-CCAATGTTATGGTCGTTGCTCA-3'
mMta2-RT-F1	5'-GCAATCCTTACCTGGTTAGACG-3'
mMta2-RT-R1	5'-TGGCTGGTAATGATTCAAACTG-3'
mHprt-RT-F	5'-AGTCCCAGCGTCGTGATTAG-3'
mHprt-RT-R	5'-TTTCCAAATCCTCGGCATAATGA-3'
mGapdh-RT-F	5'-TGTGTCCGTCGTGGATCTGA-3'
mGapdh-RT-R	5'-CCTGCTTCACCACCTTCTTGA-3'
mAdcy6-RT-F1	5'-TGAGTCTTCTAGCCAGCTCTG-3'
mAdcy6-RT-R1	5'-CAGCACCAAGTAGGTGAACCC-3'
mCcnd2-RT-F1	5'-GAGTGGGAACTGGTAGTGTTG-3'
mCcnd2-RT-R1	5'-CGCACAGAGCGATGAAGGT-3'
mCox6a2-RT-F1	5'-CTGCTCCCTTAACTGCTGGAT-3'
mCox6a2-RT-R1	5'-GATTGTGGAAAAGCGTGTGGT-3'
mErf-RT-F	5'-GGTTTGCCTTCCCAGATTGG-3'
mErf-RT-R	5'-CCTGGTACTCCTCTTTCCGAA-3'
mH1f0-RT-F	5'-CACGGACCACCCCAAGTATTC-3'

mH1f0-RT-R	5’-ACCCACCTTGTAGTGGCTCT-3’
mIkbke-RT-F	5’-ACCACTAACTACCTGTGGCAT-3’
mIkbke-RT-R	5’-CCTCCCCGGATTTCTTGTTTC-3’
mLat-RT-F	5’-ATGGAAGCAGACGCCTTGAG-3’
mLat-RT-R	5’-TGCTGTCATAGGAGACTGGCA-3’
mPadi3-RT-F	5’-CTACAGAGGATTGTGCGTGTG-3’
mPadi3-RT-R	5’-AGGAACCGCCCCATAAATGTC-3’
mRcn3-RT-F	5’-GGAATTTCCAGTACGACCATGAG-3’
mRcn3-RT-R	5’-GATCCATGCGGTCTACGATCC-3’
mTrim63-RT-F	5’-GTGTGAGGTGCCTACTTGCTC-3’
mTrim63-RT-R	5’-TGAGAGATGATCGTCTGCACT-3’
mWnt10b-RT-F1	5’-GCGGGTCTCCTGTTCTTGG-3’
mWnt10b-RT-R1	5’-CCGGGAAGTTTAAGGCCCAG-3’
Primers for mouse Ig light chain genes	
Jκ1 R	5’-CAGGATCCTAGGACAGTCAGTTTGGT-3’
Jκ2 R	5’-TTTCCAGCTTGGTCCCCCCTCCGAA-3’
Jκ4 R	5’-TTCACACAAGTTACCCAAACAG-3’
Jκ5 R	5’-TGCCACGTCAACTGATAATGAGCCCTCTC-3’
Vk universal F	5’-TGCAGSTTCAGTGGCAGTGGRTCWGGR-3’
Vλ1,2 F	5’-AGAAGCTTGTGACTCAGGAATCTGCA-3’
Jλ 2,3 R	5’-CAGGATCCTAGGACAGTGACCTTG-3’
Primers for mouse Ig heavy chain genes	
D_H F	5’-GGAATTCGMTTTTTGTSAAGGGATCTACTACTG TG-3’
V_HQ52 F	5’-CGGTACCAGACTGARCATCASCAAGGACAAYTCC-3’
V_HJ588 F	5’-CGAGCTCTCCARCACAGCCTWCATGCARCTCARC-3’
V_HJ7183 F	5’-CGGTACCAAGAASAMCCTGTWCCTGCAAATGASC-3’
J_H3 R	5'-GTCTAGATTCTCACAAGAGTCCGATAGACCCTGG-3'
Primers for testing *Mta2* gene deletion efficiency	
mMta2-E6-F	5’-GGTTGCAAATTCCAAGCTGAG-3’
mMta2-In6-R	5’-TCCACACTGGTACCCCAAATC-3’
Primers for mouse genotyping	
mMta2-40-F	5'-GCTGAAGCAGACAGCAAAC-3'
mMta2-43-R	5'-CATGCCAGGTTTTGAACCC-3'
mMta2-INF3-F	5'-CAGGGGAACAATGCACCG-3'

Primers mMta2-40-F and mMta2-43-R will produce a 335bp band for wild type Mta2 allele, and a 390 bp band for floxed Mta2 allele.
Primers mMta2-INF3-F and mMta2-43-R will produce a 360 bp band for Mta2 null allele.

mOcaB-In2-F	5'-AAACACCCATCCTGGTCTTCTT-3'
mOcaB-In2-R	5'-GACCCAGTAACCATGGAAATCA-3'
mNeo-OcaB-F	5'-CTTGTCGATCAGGATGATCTG-3'
mNeo-OcaB-R	5'-TGCACTGGAAAAGGAAATCTCA-3'

Primers mOcaB-In2-F and mOcaB-In2-R will produce a 528 bp band for wild type Oca-B allele.
Primers mNeo-OcaB-F and mNeo-OcaB-R will produce an about 1100 bp band for Oca-B null allele.